

Cite this: *J. Mater. Chem. A*, 2022, 10, 1682

## Synthetic solid oxide sorbents for CO<sub>2</sub> capture: state-of-the art and future perspectives

Ribooga Chang,<sup>†a</sup> Xianyue Wu,<sup>†bc</sup> Ocean Cheung<sup>†\*a</sup> and Wen Liu<sup>†\*b</sup>

Carbon capture is an important and effective approach to control the emission of CO<sub>2</sub> from point sources such as fossil fuel power plants, industrial furnaces and cement plants into the atmosphere. For an efficient CO<sub>2</sub> capture operation, many aspects of the CO<sub>2</sub> capture steps need to be carefully considered. Currently the most mature CO<sub>2</sub> capture technology is liquid amine scrubbing. Alternatively, solid sorbents can be used to effectively capture CO<sub>2</sub> while alleviating the disadvantages associated with liquid amine sorbents. In this review, we critically assess solid metal oxide CO<sub>2</sub> sorbents, especially oxides of group 1 (Li, Na and K) and group 2 (Mg, Ca, Sr and Ba) metals, for capturing CO<sub>2</sub> at moderate to high temperatures. In particular, we focus on the recent advances in developing synthetic metal oxide sorbents, and the correlation between the design, synthetic approaches and their cyclic CO<sub>2</sub> capture performance, which are characterised by CO<sub>2</sub> uptake capacity, rate of carbonation and cyclic stability. The state-of-the-art, challenges, opportunities and future research directions for these metal oxide sorbents are discussed. By devoting more research effort to address the issues identified, there can be great potential to utilise Group 1 and 2 metal oxides as cost-effective, highly efficient sorbents for CO<sub>2</sub> capture in a variety of carbon capture applications.

Received 7th September 2021  
Accepted 19th December 2021

DOI: 10.1039/d1ta07697c

rsc.li/materials-a

<sup>a</sup>Department of Materials Science and Engineering, Nanotechnology and Functional Materials, Uppsala University, SE75121, Sweden. E-mail: ocean.cheung@angstrom.uu.se

<sup>b</sup>School of Chemical and Biomedical Engineering, Nanyang Technological University, 62 Nanyang Drive, 637459, Singapore. E-mail: wenliu@ntu.edu.sg

<sup>c</sup>Interdisciplinary Graduate Programme, Nanyang Environmental & Water Research Institute, 1 Cleantech Loop, 637141, Singapore

† These authors contributed equally to this work.



Ribooga Chang is a PhD student at the Department of Materials Science and Engineering at Uppsala University, Sweden. Ribooga holds a master's degree from Gwangju Institute of Science and Technology (GIST), Korea. Her PhD work has been focused on the development of high-temperature sorbents and porous materials for a number of applications e.g. gas separation, water treatment, and drug delivery.



Xianyue Wu is a doctoral student in Chemical Engineering at the School of Chemical and Biomedical Engineering, Nanyang Technological University. Xianyue is also enrolled on an Interdisciplinary Graduate Programme in collaboration with Nanyang Environment & Water Research Institute (NEWRI), Residues, Resource and Reclamation Centre (R3C). She has a Bachelor of Engineering (Chemical and Biomolecular Engineering) with Honours (Highest Distinction) degree from Nanyang Technological University, Singapore. Her research interests include catalyst and process development in thermal catalysis of carbon monoxide and carbon dioxide. She is currently focusing on work regarding nickel-based dual function material for CO<sub>2</sub> capture and conversion.



# 1 Introduction

## 1.1 Background

Global warming is one of the major challenges of the present century.<sup>1</sup> The high concentration of CO<sub>2</sub> in the atmosphere due to human activity is indisputably the main cause of global warming. In particular, the combustion of fossil fuels for electricity generation, transportation, oil refining, cement production and metallurgy results in the release of CO<sub>2</sub> into the atmosphere at a rate that is far beyond what the ecosystem can take up.<sup>2</sup> Therefore, decarbonisation technologies have been one of the focal points of research in science and engineering. In a sustainable and low-carbon future, renewable energies will eventually replace fossil fuels. In the meantime, the carbon capture, storage and utilisation scheme (CCSU) will play an important role as a transitional solution to provide low-emission hydrogen, electricity and CO<sub>2</sub>-derived products from fossil fuel feedstocks. After renewable energies have completely decarbonised the energy sector, CCSU will continue to be relevant to industrial processes such as steelmaking and cement production.<sup>3</sup>

The first step in CCSU is the capture of CO<sub>2</sub> from point sources of emissions or, in the case of direct air capture (DAC), from the atmosphere. When capturing from the combustion of fossil fuels, three main strategies exist: pre-combustion, post-combustion and oxy-fuel combustion. Pre-combustion capture involves extracting CO<sub>2</sub> from syngas during hydrogen production (by gasification, reforming and downstream purification processes), followed by the combustion of the “blue hydrogen” produced. Post-combustion capture is an end-of-pipe strategy that extracts CO<sub>2</sub> from the combustion flue gases. Oxy-fuel combustion proceeds by burning carbonaceous fuels in the absence of nitrogen. The flue gas of oxy-fuel combustion, after the removal of water, NO<sub>x</sub>, SO<sub>x</sub> and any residue N<sub>2</sub>, can be considered captured. The interested reader is referred to Stanger *et al.*<sup>4</sup> for detailed discussions of various carbon capture strategies.

Regardless of the strategy, CO<sub>2</sub> capture requires gas separation, which can be achieved by various technologies including chemical scrubbing, physical adsorption (physisorption), cryogenic distillation, membrane separation, *etc.* Currently, chemical scrubbing using amine solutions is the most mature carbon capture technology, which can be deployed at commercially viable scales.<sup>5</sup> However, CO<sub>2</sub> capture by amine scrubbing is energy intensive (typically 4–6 MJ kg<sup>-1</sup> CO<sub>2</sub> captured by monoethanolamine).<sup>6</sup> In addition, liquid amine solutions are expensive to produce, corrosive, and suffers from thermal and oxidative degradation during regeneration (although some priority amine formulations claim superior cyclic stability).<sup>7</sup>

Physical sorption processes utilise sorbents in either liquid form (*e.g.* selexol) or solid form (*e.g.* zeolites and metal-organic framework) and do not require high operating temperatures.<sup>8,9</sup> Instead, the regeneration of physical sorbents requires strong vacuum and/or gentle heating, which are associated with unrecoverable energy penalty. Physisorbents such as zeolites, zeotypes, metal-organic frameworks (MOFs) tend to perform best at ambient temperatures with respect to CO<sub>2</sub> uptake capacity: zeolites and zeotype typically have high CO<sub>2</sub> uptake at low pressures in the range of approximate 4–25 wt% up to 1 bar at ambient temperatures.<sup>10</sup> MOFs perform comparably better at high pressures, CO<sub>2</sub> uptake at ambient temperatures of well over 100 wt% have been reported close to the saturation pressure of CO<sub>2</sub> (*e.g.* NU-1000).<sup>11,12</sup> It is important to note that these physisorbents do not have high CO<sub>2</sub> uptake at high temperatures (*i.e.* the temperature of combustion flue gas) and therefore, the possible use of physisorbents in CO<sub>2</sub> will require cooling of the flue gas. In addition, most physical sorption technologies are not specifically selective towards CO<sub>2</sub> and must operate under dry conditions to avoid water competing for adsorption sites. This need to de-humidify the gas feed adds extra costs. Although hydrophobic sorbents have been developed to tackle the problem associated with selectivity towards water,<sup>13,14</sup> there remains a need to reduce the production cost of these complex synthetic sorbents. As an alternative, cryogenic separation technologies



*Ocean Cheung is an assistant professor at the Division of Nanotechnology and Functional Materials at Uppsala University, Sweden. He holds a Master of Chemistry (MChem) degree from the University of Warwick, UK and a PhD in Materials Chemistry from Stockholm University, Sweden. His research is focused on the development of functional porous materials for environmental and bio-applications.*

*Focused application areas within Dr Cheung's research include gas/vapour adsorption/separation, catalysis water treatment, and controlled drug delivery.*



*Wen Liu completed his training as a chemical engineer at the University of Cambridge. He is currently an Assistant Professor at the School of Chemical and Biomedical Engineering, Nanyang Technological University. Dr Liu's research focuses on studying carbon capture and utilisation (CCU) processes, from understanding the atomic scale reaction mechanisms, to designing new CCU strategies*

*using process intensification strategies. He has a special interest in using hypothesis-driven methods to develop high performance oxide materials for carbon capture, oxygen transport, thermochemical water splitting and heterogeneous catalysis.*



exploit the difference in the boiling points of the gas molecules, such that CO<sub>2</sub> can be extracted from the process gas mixtures *via* distillation or anti-sublimation.<sup>15</sup> Therefore, cryogenic separation is capable of producing CO<sub>2</sub> of very high purity that can be readily transported and utilised without further processing. However, the supply of cryogenic chill is often costly, both in terms of capital expenditure (CAPEX) and operational costs (OPEX), unless a low-cost cold energy source (*e.g.* the latent heat of the vapourisation of liquified nature gas) is available.<sup>16</sup>

Membrane technology offers process simplicity and scalability for extracting CO<sub>2</sub> from gas mixtures.<sup>17</sup> Unfortunately, the requirement for high pressure gradients across the membranes and the low durability of the membrane materials present notable technical challenges to the large-scale deployment of membrane-based for CO<sub>2</sub> capture technologies.<sup>18</sup>

In order to address the practical issues (*e.g.* thermal degradation and corrosiveness) associated with liquid amine scrubbing, the use of solid sorbents, such as solid amines and alkali metal oxides, has been proposed. In the latter case, the solid oxide sorbents occupy a large compositional space with versatile chemical formulations that can be tailored for a variety of CO<sub>2</sub> capture applications.<sup>19</sup> For example, the temperatures at which the sorbents take up and release CO<sub>2</sub> can be tuned by design. Different types of sorbents (*e.g.* physisorbents, liquid absorbents and high temperature solid sorbents) take up CO<sub>2</sub> *via* different mechanisms and have different operational conditions, it is therefore, not always possible to compare the different types of sorbents directly. Here, we review the recent developments of solid oxide sorbents, with a focus on synthetic strategies towards improved CO<sub>2</sub> capture performance.

## 1.2 Reversible CO<sub>2</sub> uptake by metal oxide sorbents

Metal oxides capable of chemically taking up CO<sub>2</sub> typically contain alkali metals and, or alkaline earth metals. The

reversible capture of CO<sub>2</sub> by the metal oxide sorbents can be generalized by:



where  $x = 1$  and 2 for alkaline earth metals and alkaline metals, respectively. The forward reaction involves carbonating the sorbent in flue gases with typical CO<sub>2</sub> mole fractions in the range of 3–20%. The carbonation takes place in the carbonator exothermically at a low temperature, at which the equilibrium CO<sub>2</sub> partial pressure is below 0.001 bar, such that almost all the CO<sub>2</sub> in the gas stream can be cleaned up by the sorbent. The reverse reaction (*i.e.* sorbent regeneration) involves decomposing the carbonate produced in virtually pure CO<sub>2</sub>, such that the gaseous product is also a stream of pure CO<sub>2</sub>, which can be further purified and compressed for storage and, or utilisation. The regeneration takes place endothermically at a high temperature, at which the equilibrium CO<sub>2</sub> partial pressure of the reaction system exceeds 1 bar, so all of the carbonated sorbent would irreversibly decompose. Plots of the equilibrium partial pressures of CO<sub>2</sub> for the carbonation of the binary oxides of alkali metals and alkaline earth metals are shown in Fig. 1a. Note that Fig. 1a excludes elements that are either deemed too expensive (*viz.* Rb<sub>2</sub>O and CsO) or having considerable radioactivity (*viz.* Fr<sub>2</sub>O and RaO). Based on the equilibrium temperatures for reversible CO<sub>2</sub> capture and regeneration, we define three types of solid oxide sorbents: (i) CaO, which reversibly takes up CO<sub>2</sub> at high temperatures, (ii) MgO, which reversibly takes up CO<sub>2</sub> at near-ambient temperatures, and (iii) all other oxides (Li<sub>2</sub>O, Na<sub>2</sub>O, K<sub>2</sub>O, SrO and BaO), which are very strong bases whose carbonates require impractically high temperatures (*e.g.* above the melting point of the carbonates) to decompose. The ease to decompose the carbonates (as depicted in Fig. 1a) correlates well to the optical basicity of the binary



Fig. 1 (a) Equilibrium curves of partial pressures of CO<sub>2</sub> for the carbonation of the binary oxides of alkali metal/alkaline earth metal as functions of temperature. The red shaded area indicates CO<sub>2</sub> partial pressures that are practically achievable in a continuous CO<sub>2</sub> capture system. The discontinuities of the equilibrium curves changing from solid lines to dashed represents the melting point of the corresponding carbonates. (b) Schematic illustration of post-combustion CO<sub>2</sub> capture by solid sorbents in interconnected fluidised beds.





Table 1 Optical basicity of oxides based sorbents<sup>23,24</sup>

| Cation           | Oxide             | Basicity |
|------------------|-------------------|----------|
| Mg <sup>2+</sup> | MgO               | 0.78     |
| Ca <sup>2+</sup> | CaO               | 1.0      |
| Li <sup>+</sup>  | Li <sub>2</sub> O | 1.0      |
| Sr <sup>2+</sup> | SrO               | 1.1      |
| Ba <sup>2+</sup> | BaO               | 1.15     |
| Na <sup>+</sup>  | Na <sub>2</sub> O | 1.15     |
| K <sup>+</sup>   | K <sub>2</sub> O  | 1.4      |

metal oxides, as shown in Table 1, *i.e.* the carbonates derived from oxides with high optical basicity are generally hard to decompose during regeneration. Therefore, the basicity of type (iii) oxides are often chemically modified to enable reversible CO<sub>2</sub> uptake under practically accessible conditions.

As there is a temperature gap between the carbonation and the calcination steps, continuous CO<sub>2</sub> capture typically requires circulating the sorbents between two reactors, *viz.* a carbonator and a calciner. A common reactor configuration to achieve the swings between carbonation and regeneration is a set of interconnected fluidised beds, as depicted in Fig. 1b.<sup>20–22</sup>

Microscopically, the solid oxide sorbent particles undergo significant morphological changes as they cyclically take up and release CO<sub>2</sub>. Although the carbonation of different types of sorbents follows different reaction mechanisms, there are some commonalities. During CO<sub>2</sub> capture, the sorbent typically develops a layer of carbonate, restricting the access of CO<sub>2</sub> to the unreacted oxides, thus reducing the overall rates of CO<sub>2</sub> uptake. In addition, the carbonates formed generally have low melting points, causing the sorbents to sinter, thereby hindering their performance in subsequent capture cycles. Because of these limitations, there are considerable gaps between the sorbents' stoichiometric CO<sub>2</sub> uptake capacities and those practically accessible after multiple carbon capture cycles. To improve the overall efficiency and effectiveness of the oxide-based CO<sub>2</sub> capture processes, a significant amount of research is required to understand the sorbent behaviour and subsequently to rationally design high performance sorbents, often by optimising the synthesis approach. In general, an ideal solid oxide sorbent should (i) be able to undergo reversible carbonation at temperatures that are closely matching the temperatures of the upstream/downstream processes, (ii) have fast uptake and release kinetics, (iii) exhibit stable performance over large number of CO<sub>2</sub> capture cycles, (iv) have sufficient physical hardness to survive prolonged attrition in circulating fluidised beds and (v) can be produced in large quantities with relatively simple methods and low costs.

### 1.3 Objective and review outline

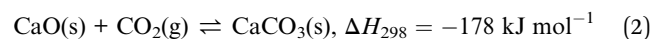
Over the past decades, there have been large number of studies that develop and investigate solid oxide CO<sub>2</sub> sorbents, with focuses on both the process and materials aspects. The interested reader is referred to past reviews which provide broad overviews of CO<sub>2</sub> capture technologies employing solid sorbents,<sup>25</sup> and in particular metal oxide-based solid sorbents.<sup>26</sup>

It is worth noting that the studies addressing the materials challenge ubiquitously point towards the need to develop high-performance synthetic sorbents. Despite the abundant reports of synthetic sorbents showing improvements over natural sorbents such as limestone, the relationships between the sorbents' compositions, synthesis methods, structures and CO<sub>2</sub> capture behaviour are still not fully understood. Therefore, given the rapid development in characterisation techniques and synthesis methods, we see the need for a critical assessment of the literature focusing the recent advances in synthetic strategies for preparing high performance metal oxide based CO<sub>2</sub> sorbents with the following specific objectives:

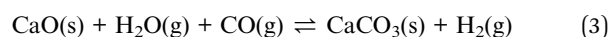
- Review the state-of-the-art understanding of the behaviour of the oxide sorbents over CO<sub>2</sub> capture cycles.
- Review different synthetic approaches for preparing high performance oxide sorbents.
- Identify knowledge gaps in understanding the behaviour of synthetic sorbents under realistic CO<sub>2</sub> capture conditions.
- Highlight emerging approaches for improving the performance of synthetic sorbents.
- Promote the need for standards for evaluating the performance of newly developed CO<sub>2</sub> sorbents.

## 2 CaO based sorbents

CaO based sorbents are the most commonly discussed due to their high CO<sub>2</sub> uptake capacity, fast carbonation and regeneration rates, high earth-abundance and low cost. In Table 2 we summarise the CO<sub>2</sub> uptake properties of a number of recently reported CaO based CO<sub>2</sub> sorbents. The reversible reaction between CaO and CO<sub>2</sub> is also known as calcium looping or calcium carbonate looping:



The forward reaction typically takes place around 650 °C, whereas regeneration takes place in 1 bar CO<sub>2</sub> at >900 °C.<sup>4</sup> The CaO sorbents can be applied to both pre- and post-combustion CO<sub>2</sub> capture at power stations, as well as CO<sub>2</sub> capture from industrial processes such as cement production.<sup>27,28</sup> In the case of pre-combustion capture,<sup>29</sup> CaO facilitates the sorbent-enhanced water gas shift to produce highly concentrated H<sub>2</sub>:<sup>30</sup>



In addition, CaO based sorbents can be used for capturing CO<sub>2</sub> produced by cement plants.<sup>31</sup> In fact, CaO based capture process can be efficiently integrated into the cement production process,<sup>32</sup> requiring only minor modifications to the existing equipment and process, whilst reducing the fuel consumption and CO<sub>2</sub> emissions by ~75% and ~85%, respectively.<sup>33</sup> Because of the relative ease to prepare CaO based sorbents at large batches, the integration of CaO based carbon capture has been demonstrated at pilot scales (to up 1.9 MWh) by various research groups.<sup>34,35</sup> Freshly prepared CaO sorbents, without any further modification, could easily take up CO<sub>2</sub> close to the



Table 2 Various reaction conditions and capacities of CaO based sorbents<sup>a</sup>

| Sorbent   | Conditions  |   |               |        |                              |                              |                        |                        |                     |                                       | Capacity                     |                               |                              |      |
|---|---|---|---------------|--------|------------------------------|------------------------------|------------------------|------------------------|---------------------|---------------------------------------|------------------------------|-------------------------------|------------------------------|------|
|   | Base (B)  | Support (S)   | Fraction of S | Method | Carbonation temperature [°C] | Calcination temperature [°C] | Carbonation time [min] | Calcination time [min] | CO <sub>2</sub> [%] | BET [m <sup>2</sup> g <sup>-1</sup> ] | CO <sub>2</sub> uptake [wt%] | CO <sub>2</sub> uptake [mol%] | Cycle capacity [loss%/cycle] | Ref. |
| S20-4x  | Ca(NO <sub>3</sub> ) <sub>2</sub> ·4H <sub>2</sub> O  | Zr(NO <sub>3</sub> ) <sub>2</sub> ·6H <sub>2</sub> O  | 0.1           | e      | 675                          | 850                          | 20                     | 10                     | 20                  | 12                                    | 41.8                         | 53.3                          | 0.8/20                       | 53   |
| S20-6x  | Ca(NO <sub>3</sub> ) <sub>2</sub> ·4H <sub>2</sub> O  | Zr(NO <sub>3</sub> ) <sub>2</sub> ·6H <sub>2</sub> O  | 0.1           | e      | 675                          | 850                          | 20                     | 10                     | 20                  | 20                                    | 49.7                         | 63.4                          | 7.3/20                       | 53   |
| S20-8x  | Ca(NO <sub>3</sub> ) <sub>2</sub> ·4H <sub>2</sub> O  | Zr(NO <sub>3</sub> ) <sub>2</sub> ·6H <sub>2</sub> O  | 0.1           | g      | 675                          | 850                          | 20                     | 10                     | 20                  | 23                                    | 48.9                         | 62.2                          | 5.7/50                       | 53   |
| CL-CE-75  | Calcium l-lactate hydrate   | CaO·Al <sub>2</sub> O <sub>3</sub> cement             | 0.25          | f      | 650                          | 900                          | 30                     | 10                     | 15                  | —                                     | 36                           | 45.9                          | —/70                         | 74   |
| CC-AN-80  | Ca <sub>3</sub> (C <sub>6</sub> H <sub>5</sub> O <sub>7</sub> ) <sub>2</sub> ·4H <sub>2</sub> O | Al(NO <sub>3</sub> ) <sub>3</sub>                     | b             | 650    | 800                          | 30                           | 10                     | 15                     | 10                  | 59                                    | 75.2                         | 14/28                         | 75                           |      |
| CaO-SBA15   | Ca(CH <sub>3</sub> COO) <sub>2</sub>  | SBA   | 0.5           | b      | 700                          | 910                          | 60                     | 30                     | 100                 | 155                                   | 43.1                         | 55                            | 20/40                        | 76   |
| CaO-CC  | CaCO <sub>3</sub>   | —   | —             | —      | 650                          | 120                          | 950                    | 30                     | 15                  | 1                                     | 71.2                         | 90.7                          | 23.75/11                     | 77   |
| CaO-ES  | CaCO <sub>3</sub>   | MgCO <sub>3</sub>                                     | —             | —      | 650                          | 120                          | 950                    | 30                     | 15                  | 1                                     | 61.8                         | 78.8                          | 20.41/11                     | 77   |
| CaO-P   | CaCl <sub>2</sub>   | —   | —             | c      | 650                          | 120                          | 950                    | 30                     | 15                  | 5                                     | 48.6                         | 61.9                          | 2.97/11                      | 77   |
| Ca-Al-CO <sub>3</sub>                                 | CaO   | Al <sub>2</sub> O <sub>3</sub>                        | 0.5           | c      | 600                          | 700                          | 45                     | 20                     | 50                  | —                                     | 55.7                         | 71                            | —/10                         | 66   |
| Ca-Al-CO <sub>3</sub>                                 | CaO   | Al <sub>2</sub> O <sub>3</sub>                        | 0.5           | c      | 600                          | 700                          | 25                     | 20                     | 50                  | —                                     | 56.7                         | 72.3                          | —/30                         | 66   |
| Ca <sub>1</sub> Ni <sub>0.1</sub>                     | Ca(NO <sub>3</sub> ) <sub>2</sub> ·4H <sub>2</sub> O  | Ni(NO <sub>3</sub> ) <sub>2</sub> ·6H <sub>2</sub> O  | 0.1           | d      | 650                          | 650                          | 25                     | 3                      | 15                  | 13                                    | 66.0                         | 84.1                          | —/20                         | 55   |
| Ca <sub>1</sub> Ni <sub>0.1</sub> Ce <sub>0.033</sub> | Ca(NO <sub>3</sub> ) <sub>2</sub> ·4H <sub>2</sub> O  | Ce(NO <sub>3</sub> ) <sub>2</sub> ·6H <sub>2</sub> O  | 0.033         | d      | 650                          | 650                          | 25                     | 3                      | 15                  | 21                                    | 62.1                         | 79.1                          | —/20                         | 55   |
| CNAN-SG   | Ca(NO <sub>3</sub> ) <sub>2</sub> ·4H <sub>2</sub> O  | Al(NO <sub>3</sub> ) <sub>3</sub> ·9H <sub>2</sub> O  | 0.3           | d      | 650                          | 900                          | 5                      | 5                      | 15                  | 13                                    | 27.5                         | 35                            | 28/21                        | 65   |
| CAAN-SG   | Ca(CH <sub>3</sub> COO) <sub>2</sub>  | Al(NO <sub>3</sub> ) <sub>3</sub> ·9H <sub>2</sub> O  | 0.3           | d      | 650                          | 900                          | 5                      | 5                      | 15                  | 12                                    | 13.6                         | 17.3                          | 40/21                        | 65   |
| CaO-GS 2 mM   | CaO   | Gemini surfactant                                     | 0.0008        | f      | 600                          | 850                          | —                      | 30                     | 15                  | 16                                    | 29.0                         | 37                            | —                            | 72   |
| CaO-SDS 20 mM   | CaO   | Sodium dodecyl sulfate                                | 0.008         | f      | 600                          | 850                          | —                      | 30                     | 15                  | 9                                     | 27.0                         | 34.4                          | —                            | 72   |
| CaO-(s-s)   | CaO   | ZrO <sub>2</sub>                                      | 0.03          | e      | 650                          | 780                          | 120                    | 60                     | Pure                | —                                     | 57.7                         | 73.5                          | —                            | 58   |
| CaO-(c-sg)  | CaO   | ZrO <sub>2</sub>                                      | 0.03          | d      | 650                          | 780                          | 120                    | 60                     | Pure                | —                                     | 77.5                         | 98.7                          | —                            | 58   |
| CaO/CaZrO <sub>3</sub>                                | Ca(NO <sub>3</sub> ) <sub>2</sub> ·4H <sub>2</sub> O  | ZrO(NO <sub>3</sub> ) <sub>2</sub> ·xH <sub>2</sub> O | 0.14          | d      | 650                          | 850                          | 30                     | 5                      | 15                  | —                                     | ~48.0                        | 61.1                          | 7/50                         | 68   |
| CaO-ZrO <sub>2</sub> -SG                              | CaO   | ZrO <sub>2</sub>                                      | 0.1           | d      | 200                          | 900                          | —                      | —                      | —                   | 25                                    | 65.0                         | 82.8                          | —/20                         | 59   |
| CaO-ZrO <sub>2</sub> -IM                              | CaO   | ZrO <sub>2</sub>                                      | 0.1           | b      | 200                          | 900                          | —                      | —                      | —                   | 19                                    | 64.0                         | 81.6                          | 6.25/14–20                   | 59   |
| Ca-hyd_95:5_2 h                                       | Ca(OH) <sub>2</sub>   | ZrO <sub>2</sub>                                      | 0.05          | d      | 800                          | 800                          | 5                      | 15                     | 50                  | 12                                    | 51.0                         | 65                            | 39.22/90                     | 78   |
| Ca-hyd_95:10_2 h                                      | Ca(OH) <sub>2</sub>   | ZrO <sub>2</sub>                                      | 0.1           | d      | 750                          | 750                          | 20                     | 10                     | 40                  | 11                                    | 52.0                         | 66.3                          | 5.77/10                      | 78   |
| C74D26  | Carbide   | Dolomite  | 0.35          | a      | 700                          | 850                          | 20                     | 10                     | 15                  | 14                                    | 54.0                         | 68.9                          | —/10                         | 79   |
| Mg/Ca-0.2   | Ca(CH <sub>3</sub> COO) <sub>2</sub>  | Mg(NO <sub>3</sub> ) <sub>2</sub>                     | 11            | d      | 700                          | 700                          | 30                     | 30                     | Pure                | —                                     | 59.2                         | 75.4                          | 4.7/7                        | 80   |
| Ca/Al-2.5-1%  | CaO   | Al <sub>2</sub> O <sub>3</sub>                        | 0.4           | c      | 600                          | 700                          | 45                     | 20                     | 100                 | 6                                     | 59.1                         | 75.3                          | 5.9/220                      | 48   |
| Ca-CNT  | CaO nanotube  | —   | —             | —      | 650                          | 850                          | 30                     | 10                     | 15                  | 12                                    | 58.0                         | 73.9                          | 34.48/15                     | 81   |

<sup>a</sup> (a) Combustion, (b) impregnation, (c) precipitation, (d) sol-gel, (e) solid-state, (f) wet-mixing, (g) solution-combustion.

stoichiometric capacity of 78 wt% (based on the mass of the fully calcined CaO)<sup>36,37</sup> however, the performance of unmodified CaO sorbents will rapidly deteriorate over uptake–regeneration cycles as a result of sintering,<sup>38,39</sup> as the surface area and accessible pore volumes of the sorbents rapidly diminish. In continuous operation, the deactivated sorbents act as inert materials, which imposes significant energy penalty as they participate in the temperature swing cycles without capturing CO<sub>2</sub>. The deactivation mechanism during calcium looping cycles has been extensively studied.<sup>32,40–42</sup> The biggest challenge of using CaO sorbents is to develop solutions that address their poor cyclic stability. The two general strategies to improve the performance of calcium looping systems are (i) optimising operating conditions and (ii) prepare high performance synthetic sorbents, as discussed in the following sections.

### 2.1 Optimising operating conditions

The performance of the CaO based sorbents depends on the operating conditions. Accordingly, researchers have exploited such dependence to delay or mitigate sorbent deactivation over calcium looping cycles. For example, the presence of steam in the calcium looping reactors is found to influence both reaction rates and mass transfer<sup>43,44</sup> specifically, steam is known to enhance the rate of calcination.<sup>45,46</sup> In addition, experimental observations suggest that operation in the presence of steam increases the porosity of the sorbents, and subsequently improve their CO<sub>2</sub> capture performance in terms of both reaction kinetics and cyclic stability.<sup>47,48</sup>

The issue of sorbent deactivation can also be circumvented by reactivating the spent sorbents. The recent study by Sun *et al.*<sup>49</sup> provided insights into the effects of different reactivation methods on the cyclic performance of CaO/MgO (CaO : MgO mass ratio = 75 : 25) sorbents, obtained using calcium acetate monohydrate and magnesium acetate tetrahydrate as precursors. Sun *et al.*<sup>49</sup> tested different sorbent reactivation methods: (i) hydration, (ii) hydration/impregnation and (iii) acidification. Good cyclic stability was observed when the sorbent was reactivated by hydration or hydration/impregnation, rendering CO<sub>2</sub> uptake of 39 and 41.4 wt% (49.7 and 52.8 mol%) after 40 cycles, respectively. In both cases, the CO<sub>2</sub> uptake increase with the number of cycles due to “self-activation”. Self-activation,

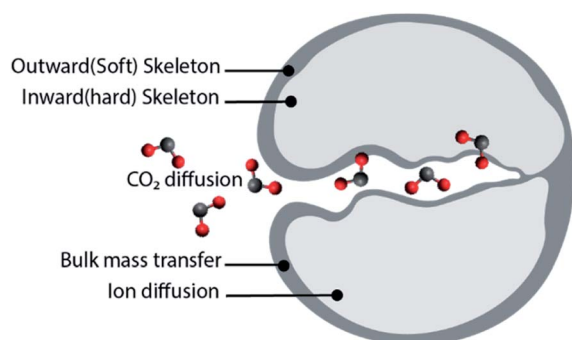


Fig. 2 The pore skeleton model for CO<sub>2</sub> and ion diffusion. Illustrated according to the finding presented in ref. 51.

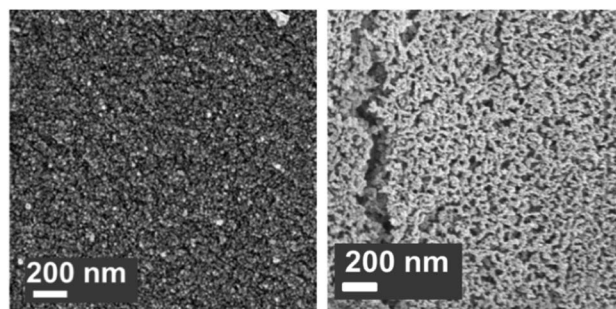


Fig. 3 Scanning electron micrograph of CaO stabilised with both MgO and Al<sub>2</sub>O<sub>3</sub> (left) as-synthesised and (right) after 23 cycles of carbonation/calcination.<sup>56</sup>

sometimes referred to as “deep carbonation”, is a phenomenon that can be explained using the pore skeleton model by Manovic and Anthony,<sup>50</sup> as depicted in Fig. 2. An inward hard skeleton is formed during calcination. However, the hard skeleton hampers the ion diffusion through the product layer of CaCO<sub>3</sub>, impeding the rate of carbonation during the initial cyclic operation. Over the carbonation–regeneration cycles, the soft skeleton is gradually activated and contributes to an increase rate of carbonation.<sup>50</sup>

Sorbent reactivation by acidification is relevant for removing the irreversibly formed CaSO<sub>4</sub> due to the presence of SO<sub>2</sub> in the flue gas. For a CaO : MgO sorbent, reactivation by acidification resulted in a CO<sub>2</sub> uptake of 23.3 wt% (29.7 mol%) after 40 cycles. Thus, acidification as a reactivation method needs further development to overcome the high cost and the potential release of toxic substances.<sup>49</sup>

### 2.2 Synthetic CaO based sorbents stabilised by inert supports

In addition to employing reactivation steps, the cyclic performance of CaO sorbents can be fundamentally improved by mixing CaO with inert refractory materials (*e.g.* Al<sub>2</sub>O<sub>3</sub>, ZrO<sub>2</sub>,

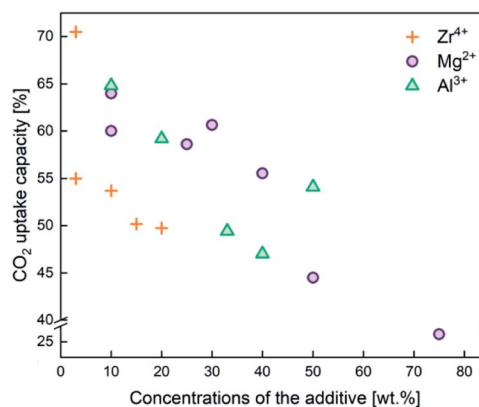


Fig. 4 CO<sub>2</sub> capture capacity of CaO based sorbents stabilised by the three different typical sintering-resistant, oxidic additives containing Zr<sup>4+</sup>, Al<sup>3+</sup>, and Mg<sup>2+</sup>. The effect of these additives on the cyclic stability of CaO sorbents is summarised in Table 2.



MgO and their derivatives) to render additional sintering resistance and physical hardness. A number of studies have reported CaO based sorbents supported on varying amounts of refractory materials. The resulting CO<sub>2</sub> uptake capacity also varied, partly due to the differences in the overall compositions, as shown in Fig. 4. The stabilising effects of adding different types and amounts of thermally stabilising cations, referencing notable recent works, are summarised in Table 2 and discussed below.

Soleimanisalim *et al.*<sup>52</sup> used CaCl<sub>2</sub>·2H<sub>2</sub>O and a small amount of ZrO(NO<sub>3</sub>)<sub>2</sub>·6H<sub>2</sub>O as precursors to prepare a stabilised CaO sorbent containing 10 wt% CaZrO<sub>3</sub> perovskite by the solution combustion method. The resulting CaO sorbent showed a high CO<sub>2</sub> uptake of ~53.3 wt% (68.2 mol%) in the first cycle and ~42.7 wt% (54.41 mol%) after 31 cycles. The stabilising effect of CaZrO<sub>3</sub> was also reported by Hashemi *et al.*<sup>53</sup> who found 20 wt% CaZrO<sub>3</sub> to be optimal for maintaining cyclic stability (46.2 wt% (58.87 mol%) after 20 cycles). To maximise cyclic stability and CO<sub>2</sub> capture performance, the type of stabiliser and the amount of stabiliser were optimized in the relevant studies.<sup>43,44</sup> Specifically, Guo *et al.*<sup>39</sup> showed that the Ca : Al ratio of Ca–Al mixed oxides (Ca<sup>2+</sup>/Al<sup>3+</sup> = 2, 2.5, 3, 3.5, 4) synthesised by coprecipitation affected the CO<sub>2</sub> uptake capacity. The Ca : Al ratio of 2.5 gave the highest CO<sub>2</sub> uptake capacity of around 47 wt% (60 mol%) after 3 cycles. The high CO<sub>2</sub> capacity and reasonable cyclic performance was attributed to the large pore size and the small particle size. Compared to the morphological properties, the amount of Ca<sub>12</sub>Al<sub>14</sub>O<sub>33</sub> present was also found to be a crucial factor in determining the sorbent's CO<sub>2</sub> capture capacity.<sup>48,52,54</sup> Sun *et al.*<sup>55</sup> revealed that CeO<sub>2</sub> can be used as an effective physical barrier to prevent the sintering of CaO. Similarly, Vall *et al.*<sup>56</sup> employed MgO and Al<sub>2</sub>O<sub>3</sub> to stabilise a synthetic CaO sorbent, obtained by calcining highly porous amorphous calcium carbonate (HPACC–BET surface area of over 450 m<sup>2</sup> g<sup>-1</sup>). Whilst MgO alone can effectively stabilise the CaO sorbent, the sorbent synergistically stabilised by both MgO and Al<sub>2</sub>O<sub>3</sub> yielded even higher stability, showing only a 2.8% decrease in the CO<sub>2</sub> uptake capacity after 23 cycles (1st cycle 54.2 wt%, 69.1 mol%). Scanning electron micrographs (SEM) (Fig. 3) of the CaO stabilised with both MgO and Al<sub>2</sub>O<sub>3</sub> confirmed the effective hinderance of sintering after 23 cycles.

**2.2.1 Preparing supported sorbents by sol–gel method.** The effective mixing between CaO and thermal stabilisers (*i.e.* support materials) is critical to enhancing the cyclic CO<sub>2</sub> capture performance. Conventional preparation methods, such as mechanical mixing, impregnation and co-precipitation may not provide sufficient dispersion of the thermal stabilisers within the sorbent matrix. To this end, sol–gel method has been explored as an alternative strategy to prepare supported CaO sorbents.<sup>57</sup> In general, sol–gel methods can induce and control the chemical interaction between the inert supports and CaO, whilst allowing the facile control of particle size and surface area. Yoon *et al.*,<sup>58</sup> Sultana *et al.*<sup>59</sup> and Gao *et al.*<sup>60</sup> all showed that CaO based sorbents prepared by sol–gel synthesis result in increased specific surface areas and pore volumes. The increased porosity can come from reduced particle size, leading to shortened CO<sub>2</sub> diffusion paths and consequently accelerated

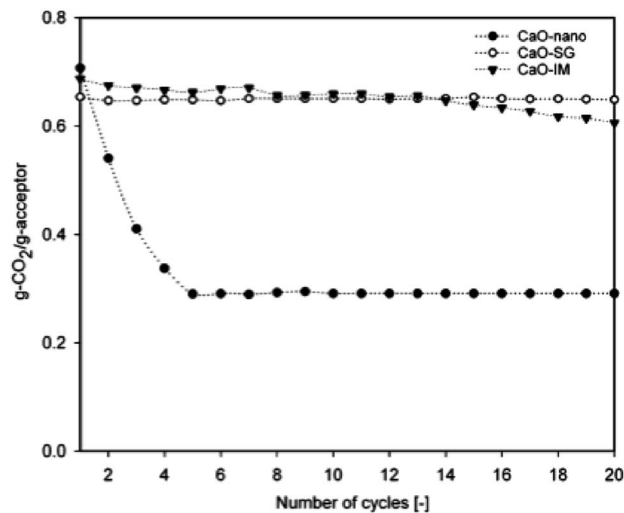


Fig. 5 CO<sub>2</sub> capture capacity of nano-CaO by sol–gel and wet impregnation methods. Reprinted with permission from ref. 59. Copyright 2021 American Chemical Society.

rate of CO<sub>2</sub> capture. For example, Zr-modified CaO prepared by Yoon *et al.*<sup>58</sup> had small particle sizes of ≤2 μm, high CO<sub>2</sub> uptake of 73.2 wt% (93.3 mol%) (compared to 54 wt% (69 mol%) of the sorbent prepared by physical mixing). In addition the CO<sub>2</sub> uptake capacity sustained at ~70.5 wt% (89.8 mol%) over 10 cycles.<sup>58</sup> Sultana *et al.*<sup>59</sup> prepared nano-CaO coated with ZrO<sub>2</sub> by sol–gel, wet impregnation, and hydrolysis methods. They found that sol–gel synthesis gave the most stable CaZrO<sub>3</sub> protective layer on the surface of the nano-CaO, with excellent CO<sub>2</sub> uptake of 65 wt% (83 mol%) after 20 cycles, as shown in Fig. 5.<sup>59</sup> Similarly, Gao *et al.*<sup>60</sup> synthesised CaO supported on charcoal by physical mixing, sol–gel, and wet impregnation and found that the CaO supported on charcoal by sol–gel method showed a high CO<sub>2</sub> capture capacity of 66.5 wt% (84.7 mol%).<sup>60</sup> In both studies, the sol–gel methods produced sorbents with the higher pore volumes, surface areas, CO<sub>2</sub> uptake and cyclic stability than sorbents prepared by other methods.

**2.2.2 Core–shell structured sorbents.** One special type of stabilised CaO based sorbents is core–shell structured sorbents, where the stabilising oxides form shells encapsulating the CaO cores. In effect, the inert shells form continuous physical barriers, preventing the cores from fusing into each other. Han *et al.*<sup>61</sup> synthesised the CaO@Al<sub>2</sub>O<sub>3</sub> core–shell structure sorbent and observed 41 wt% (52 mol%) of CO<sub>2</sub> uptake after 20 cycle with Al<sub>2</sub>O<sub>3</sub> shell thicknesses of between 4 to 8 nm. The covered cores (CaO) have resisted sintering over CO<sub>2</sub> capture cycles.<sup>61</sup> The thickness of the shell can be one of the factors determining the overall CO<sub>2</sub> capture performance. Armutlulu *et al.*<sup>62</sup> prepared CaO@Al<sub>2</sub>O<sub>3</sub> core–shell sorbents, with three different shell thicknesses. The thickness around 2.75 nm reported relatively good stability and CO<sub>2</sub> uptake capacity of ~55 wt% (70 mol%) after 30 cycles, whereas thicker Al<sub>2</sub>O<sub>3</sub> layers lead to lower initial CO<sub>2</sub> uptake.<sup>62</sup> In addition to the CaO@Al<sub>2</sub>O<sub>3</sub> design, Peng *et al.*<sup>63</sup> added TiO<sub>2</sub> as a secondary stabiliser. The resulting CaO@TiO<sub>2</sub>–Al<sub>2</sub>O<sub>3</sub> showed high stability and CO<sub>2</sub>





uptake of 46 wt% (59 mol%) after 104 cycles.<sup>63</sup> Using a 2.7 nm Al<sub>2</sub>O<sub>3</sub> coating on CaO nanoparticles, Kurlov *et al.*<sup>54</sup> demonstrated a 140% improvement in CO<sub>2</sub> uptake over a limestone reference and excellent cyclic stability (41 wt% (52 mol%) uptake after 10 cycles). They found the addition of the Al<sub>2</sub>O<sub>3</sub> layers induced the formation of inert Ca<sub>12</sub>Al<sub>14</sub>O<sub>33</sub> and Ca<sub>3</sub>Al<sub>2</sub>O<sub>6</sub> on the surface of CaO nanoparticles, produced by the calcination of calcite obtained by sacrificial template synthesis, with an average particle size of 350 nm and a BET surface area of 16 m<sup>2</sup> g<sup>-1</sup>. Consequently, the shell layer consisting of Ca<sub>12</sub>Al<sub>14</sub>O<sub>33</sub> and Ca<sub>3</sub>Al<sub>2</sub>O<sub>6</sub> acts as an effective thermal stabiliser.<sup>54</sup>

**2.2.3 Effect of synthesis parameters.** It is well established that the CO<sub>2</sub> uptake performance, including kinetics and cyclic stability, are functions of the sorbents' starting structures, which are in turn determined by the synthesis parameters used during sorbent preparation. For early literature on the synthesis of CaO based sorbents, we refer the reader to the reviews by Liu *et al.*<sup>64</sup> and Kierzkowska *et al.*<sup>29</sup> Here, we focus on recent studies (last ~5 years) investigating the effects of key synthesis parameters, as discussed in the following.

**Precursors.** Although the exact roles and effects of the various chemical precursors may differ, they are nonetheless critical to the performance of the synthesised sorbents. Azimi *et al.*<sup>65</sup> demonstrated that different combinations of Ca and Al precursors yield sorbents with noticeably different particle sizes, surface areas and morphologies. For instance, for the sol-gel synthesis of a CaO based sorbent, highly soluble nitrate precursors such as calcium nitrate (CN) and aluminium nitrate (AN) form inert phases such as Ca<sub>12</sub>Al<sub>14</sub>O<sub>33</sub> and Ca<sub>9</sub>Al<sub>6</sub>O<sub>18</sub> more easily than the nitrate-free precursors. The insoluble precursors such as nano-structured alumina (nA) formed a more compact structure than the ones prepared from aluminium nitrate (AN), which yielded a "fluffy structure" with a surface area of 13 m<sup>2</sup> g<sup>-1</sup> and a mean particle size ~16.9 nm. Overall, the Al-supported CaO sorbent synthesised with soluble nitrate precursors showed the highest CO<sub>2</sub> uptake (91.7 wt% (117 mol%), with 28 wt% loss after 21 cycles) than sorbents synthesised from other types of precursors.

**Synthesis and calcination temperatures.** Temperature is a factor that can be used to control the surface area and particle size of CaO based sorbents. Kou *et al.*<sup>66</sup> observed that high synthesis temperature promoted crystal growth and particle aggregation in Ca–Al mixed oxides. The average particle size of the samples also increased from 29.5 nm for the synthesised at RT to 42.1 nm for the sorbent synthesised at 80 °C. In fact, the crystallinities of CaO, Ca–Al spinel and CaCO<sub>3</sub> all increased with increasing synthesis temperature, as shown in Fig. 6. On the other hand, the increase in particle size is accompanied by a decrease in CO<sub>2</sub> capture capacity.

Apart from the temperature of the wet-synthesis, the calcination temperatures also affect the surface areas and pore volumes of the sorbents. Wang *et al.*<sup>67</sup> observed during the synthesis of CaO/CaZrO<sub>3</sub> hollow spheres that the heating rate of calcination significantly affected the cyclic stability of the sorbent – a slow heating rate of 5 °C min<sup>-1</sup> resulted in a stable (capacity decreased by <5 wt% after 30 cycles) compared to a sorbent prepped with a calcination rate of 20 °C min<sup>-1</sup>

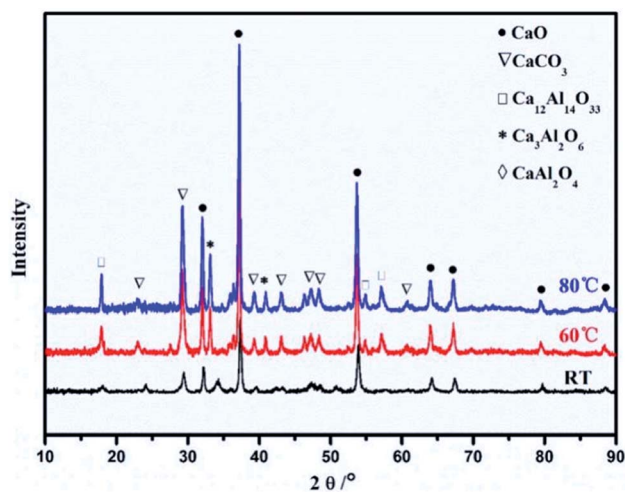


Fig. 6 XRD patterns of the Ca–Al mixed oxides ( $\text{Ca}^{2+}/\text{Al}^{3+} = 3$ ) synthesised at room temperature (RT), 60 °C and 80 °C. Reprinted with permission<sup>66</sup> copyright 2021 Elsevier.

(capacity decreased by <20 wt%).<sup>67</sup> Antzara *et al.*<sup>68</sup> performed the calcination of ZrO<sub>2</sub> promoted CaO at 750 and 800 °C and found that low calcination temperature (750 °C) reduced sintering during carbonation and resulted in CaO with high surface area and pore volume compared to CaO/ZrO<sub>2</sub> sorbents calcined at 800 °C.<sup>68</sup>

**Template.** The templated synthesis of CaO based sorbent has been adopted for morphology control and to introduce macroporosity to the sorbent. Carbon based template is one of the most commonly used for the synthesis of structured CaO sorbents. Ping *et al.*<sup>69</sup> found that the cage-like CaCO<sub>3</sub> hollow spheres synthesised using Ca(NO<sub>3</sub>)<sub>2</sub>, urea and polysaccharide spheres template showed an excellent CO<sub>2</sub> uptake of up to 78.6 wt% (100.2 mol%) in the first cycle, 45 wt% higher than the same composition synthesised without the template. Colloidal carbon spheres derived from glucose were used as the template for the synthesis of CaO/CaZrO<sub>3</sub> and CaO sorbents.<sup>67,70</sup> Wang *et al.*<sup>67</sup> found that CaO/CaZrO<sub>3</sub> hollow spheres synthesised with Ca(NO<sub>3</sub>)<sub>2</sub> and Zr(NO<sub>3</sub>)<sub>4</sub>, templated with carbon sphere (from glucose) had improved cyclic stability over 100 cycles. In a similar study, Wang *et al.*<sup>70</sup> prepared CaO based meshed hollow spheres by urea hydrolysis with carbon sphere (from glucose) template and demonstrated a high CO<sub>2</sub> capacity of ~75 wt% (96 mol%) in the first cycle, with a moderate capacity decrease of 12 wt% over 28 cycles. The authors suggested that the hollow sphere structures could produce porous CaO particles with improved CO<sub>2</sub> uptake.<sup>70</sup> In other similar studies, Naeem *et al.*<sup>71</sup> incorporated a carbon template, prepared by poly-condensation of resorcinol with an aqueous formaldehyde solution, to the sol-gel synthesis of a Al<sub>2</sub>O<sub>3</sub> and Y<sub>2</sub>O<sub>3</sub> supported CaO sorbent. The resulting structure consisting of interconnected microspheres of supported CaO had an uptake of CO<sub>2</sub> of 61 wt% (78 mol%), which remained unchanged after 10 cycles.<sup>71</sup>

**Surfactants.** Previous studies have shown the use of surfactant to be an effective way to control the particle size of CaO based sorbents. In a number of cases, such as Jamrunroj *et al.*<sup>72</sup>





Table 3 Various reaction conditions and capacities of MgO based sorbents<sup>a</sup>

| Sorbent   | Conditions   |   |                      |               |        |                              |                              |                        |                        |                     | Capacity                              |                               |                               |          |     |
|---|--|---|----------------------|---------------|--------|------------------------------|------------------------------|------------------------|------------------------|---------------------|---------------------------------------|-------------------------------|-------------------------------|----------|-----|
|   | Name of the sorbent                                  | Base (B)  | Promotor (P)         | Fraction of S | Method | Carbonation temperature [°C] | Calcination temperature [°C] | Carbonation time [min] | Calcination time [min] | CO <sub>2</sub> [%] | BET [m <sup>2</sup> g <sup>-1</sup> ] | CO <sub>2</sub> uptake [mol%] | Cycle stability [loss%/cycle] | Ref.     |     |
| MgO-AMS <sub>10</sub> -325 °C                         | MgO  | LiNO <sub>3</sub> , KNO <sub>3</sub> , Na <sub>2</sub> CO <sub>3</sub> , K <sub>2</sub> CO <sub>3</sub> | 0.44, 0.56, 0.5, 0.5 | c             | c      | 325                          | 450                          | 180                    | 90                     | HP                  | —                                     | 83.9                          | 76.8                          | 17/30    | 88  |
| MgO-AMS <sub>10</sub> -350 °C                         | MgO  | NaNO <sub>3</sub> , NaNO <sub>2</sub>   | 0.07, 0.15           | c             | c      | 350                          | 450                          | 240                    | 60                     | HP                  | —                                     | 81.5                          | 74.6                          | —        | 88  |
| MgO-NaNO <sub>3</sub> + NaNO <sub>2</sub>             | MgO  | NaNO <sub>3</sub> , NaNO <sub>2</sub>   | 0.07, 0.15           | c             | c      | 350                          | 400                          | 30                     | 20                     | Pure                | 23                                    | 55.0                          | 50.4                          | 55.2/15  | 84  |
| MgO-NaNO <sub>3</sub>                                 | MgO  | NaNO <sub>3</sub>   | 0.07                 | c             | c      | 325                          | 400                          | 30                     | 20                     | Pure                | 29                                    | 83.2                          | 76.2                          | 54.5/15  | 84  |
| MgO-K <sub>2</sub> CO <sub>3</sub>                    | Mg(NO <sub>3</sub> ) <sub>2</sub> ·6H <sub>2</sub> O | K <sub>2</sub> CO <sub>3</sub>  | 3                    | b             | b      | 375                          | 400                          | 20                     | 30                     | 100                 | 2                                     | 8.6                           | 7.8                           | 5.1/17   | 104 |
| MgO-KNO <sub>3</sub>                                  | MgO  | KNO <sub>3</sub>  | 0.2                  | c             | c      | 325                          | 450                          | 20                     | 30                     | 100                 | 107                                   | 10.2                          | 9.4                           | 2412     | 105 |
| MgO-KNO <sub>3</sub>                                  | MgO  | KNO <sub>3</sub>  | 0.2                  | c             | c      | 375                          | 450                          | 20                     | 30                     | 100                 | 107                                   | 8.3                           | 7.6                           | 10/12    | 105 |
| Na-Mg double salt                                     | MgO  | Na <sub>2</sub> CO <sub>3</sub>   | 0.1                  | a             | a      | 375                          | 500                          | —                      | —                      | Pure                | —                                     | 15.4                          | 14.1                          | 0/7      | 106 |
| MgO-Na <sub>2</sub> CO <sub>3</sub>                   | Mg(NO <sub>3</sub> ) <sub>2</sub> ·6H <sub>2</sub> O | Na <sub>2</sub> CO <sub>3</sub>   | 0.5                  | b             | b      | 380                          | 470                          | 60                     | 10                     | 100                 | —                                     | 15.0                          | 13.7                          | —/9      | 107 |
| MgONaNa-0.1   | MgO  | Na <sub>2</sub> CO <sub>3</sub> , NaNO <sub>3</sub>   | 0.1                  | b             | b      | 325                          | 450                          | 60                     | 10                     | Pure                | 39                                    | 45.2                          | 41.4                          | 34.96/14 | 91  |
| 1.00NaNO <sub>3</sub> /MgO                            | MgO  | NaNO <sub>3</sub>   | 1                    | b             | b      | 330                          | 400                          | —                      | —                      | 100                 | —                                     | 23.3                          | 21.4                          | —/15     | 108 |
| MgO-(Li/Na/K)   | MgO  | LiNO <sub>3</sub> , NaNO <sub>2</sub> , KNO <sub>2</sub>  | 0.1                  | b             | b      | 300                          | 450                          | 240                    | 60                     | HP                  | 19                                    | 73.9                          | 67.7                          | —        | 109 |
| MgO-(Li/Na/K)   | MgO  | MgO   | 0.1                  | b             | b      | 350                          | 350                          | 30                     | 30                     | HP                  | 19                                    | 14.1                          | 12.9                          | —/20     | 109 |
| MgO-(Li/Na/K)   | MgO  | MgO   | 0.1                  | b             | b      | 340                          | 450                          | 240                    | 60                     | 100                 | —                                     | 69.1                          | 63.3                          | 14/20    | 86  |
| Mg <sub>3</sub> Al <sub>1</sub> -CO <sub>3</sub> PH12 | Mg(NO <sub>3</sub> ) <sub>2</sub> ·6H <sub>2</sub> O | Al(NO <sub>3</sub> ) <sub>3</sub> ·9H <sub>2</sub> O  | 0.3                  | c             | c      | 200                          | 400                          | —                      | 60                     | —                   | —                                     | 3.7                           | 3.3                           | —        | 110 |
| NaNO <sub>3</sub> -5Mg30-MgO                          | Mg(NO <sub>3</sub> ) <sub>2</sub> ·6H <sub>2</sub> O | NaNO <sub>3</sub>   | 0.2                  | d             | d      | 300                          | 450                          | 180                    | 60                     | 100                 | —                                     | 11.5                          | 10.5                          | +19.02/8 | 111 |
| MgONaNO <sub>3</sub>                                  | Hydrotalcite   | NaNO <sub>3</sub>   | 0.2                  | d             | d      | 300                          | 450                          | 180                    | 60                     | 100                 | —                                     | 37.4                          | 34.3                          | 53.6/8   | 111 |
| MgO-10%CeO <sub>2</sub>                               | MgO-CeO <sub>2</sub>                                 | LiNO <sub>3</sub> , KNO <sub>3</sub> , Na <sub>2</sub> CO <sub>3</sub> , K <sub>2</sub> CO <sub>3</sub> | 0.17                 | a             | a      | 325                          | 425                          | 60                     | 15                     | 100                 | 252                                   | 35                            | 32.1                          | +1.22/30 | 112 |
| 5A5M  | Mg(NO <sub>3</sub> ) <sub>2</sub> ·6H <sub>2</sub> O | Al(NO <sub>3</sub> ) <sub>3</sub> ·9H <sub>2</sub> O  | 1                    | a             | a      | 200                          | 600                          | 60                     | 60                     | 10                  | 177                                   | 13.1                          | 12                            | 12/6     | 113 |
| MgO-AC  | Mg(NO <sub>3</sub> ) <sub>2</sub> ·6H <sub>2</sub> O | NH <sub>4</sub> OH  | 5                    | c             | c      | 300                          | 400                          | 60                     | —                      | UP                  | 362                                   | 5.2                           | 4.7                           | 42/27    | 96  |

<sup>a</sup> (a) Sol-gel, (b) wet mixing, (c) precipitation, (d) physical mixing, (HP) high purity, (UP) ultra purity.

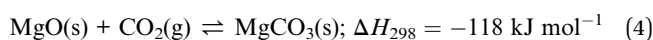
and Chen *et al.*,<sup>73</sup> there is an optimal amount of surfactant that is required to produce high performance sorbents. Jamrunroj *et al.*<sup>72</sup> found that 2 mM of gemini (GS: 12-carbon hydrophobic chains and 3 carbon alkyl spacer, 12-3-12) yielded the best CO<sub>2</sub> capture performance. The resulting CaO-GS-2 mM sorbent, having small particles of (~37 nm) and high surface area (16 m<sup>2</sup> g<sup>-1</sup>), showed the highest CO<sub>2</sub> uptake (29 wt% (37 mol%)) amongst all the CaO-GS sorbents tested.<sup>72</sup> Similarly, Chen *et al.*<sup>73</sup> concluded that the best performing CuO/CaO sorbent was obtained with a low H<sub>2</sub>O : cetyltrimethyl ammonium bromide (C<sub>19</sub>H<sub>42</sub>BrN, CTAB) molar ratio of 23 : 1. This low CTAB ratio is important for producing small particles (46.5 nm) with a CO<sub>2</sub> uptake of 13 wt% (17 mol%), which decreased to 10 wt% (13 mol%) after 19 cycles.<sup>73</sup> These studies exemplify that optimal levels of surfactant are crucial for producing sorbent materials with small particle sizes and high capture performance. However, in the case of CaO synthesised with sulphonic single chain (SDS), 40 mM of SDS yield the smallest particles with the lowest CO<sub>2</sub> uptake of 18 wt% (23 mol%) compared to other SDS doping amount.<sup>72</sup> Therefore, the surfactant effect cannot be easily generalised. In addition, factors such as the micellar structures and the interfacial adsorption ability of the surfactant should also be thoroughly understood and carefully considered during synthesis.

### 2.3 Summary and knowledge gap

CaO based CO<sub>2</sub> sorbents are promising for capturing CO<sub>2</sub> at high temperatures. These sorbents show high CO<sub>2</sub> uptake capacities with rapid uptake kinetics. Significant advances have been made to improve the performance of the sorbents through carefully tuned synthetic procedures and formulations. However, major challenges remain for the efficient, robust, long term, cost-effective application of CaO based sorbents. Besides steam injection and sorbent reactivation, there are a number of synthetic approaches to enhance the uptake and cyclic stability of CaO sorbents, primarily involving supporting CaO with thermally stable support materials and optimising synthetic parameters. Challenges lie in gaining an in-depth understanding of the effectiveness of each approach, and how they can be synergistically combined to enhance the performance of the CaO sorbents. On that front, we find the use of surfactant in the synthesis of CaO sorbents a particularly interesting avenue for further research. Making good use of surfactants' surface chemistry could hold the key to producing stable, small and porous CaO particles.

## 3 MgO based sorbents

Magnesium oxide (MgO) captures CO<sub>2</sub> by:



The reversible CO<sub>2</sub> capture can be carried out over the temperature range between 200 and 400 °C, making it suitable for heat integration with processes where abundant low-grade heat is available. Although the maximum theoretical CO<sub>2</sub> uptake by MgO sorbent is high (110 wt%, 101 mol%), the

practically accessible uptake capacity is no more than 10 wt%, owing to the formation of an impermeable layer of MgCO<sub>3</sub>, which effectively stops the encapsulated MgO from further carbonation. On the other hand, the low operating temperatures could mitigate sorbent deactivation by sintering. Therefore, the majority of the research efforts in developing synthetic MgO based sorbents focus on improving the CO<sub>2</sub> uptake capacities through physical and chemical modifications, including (i) introducing dopants to promote the reaction with CO<sub>2</sub> or (ii) preparing nanostructured MgO with very large specific surface areas to minimise the encapsulation of MgO by MgCO<sub>3</sub>. A recent review by Hu *et al.*<sup>82</sup> focuses on the development of MgO sorbent for CO<sub>2</sub> capture and provides a detailed insight in this topic. Here, we present a focused discussion on the synthesis and performance of these MgO sorbents. A list of recently developed MgO sorbents and their CO<sub>2</sub> capture performance is shown in Table 3, with key papers discussed in the following sections.

### 3.1 Promoted MgO sorbents

Recently, the used of alkali metal nitrates has been in the spotlight as a means to improve CO<sub>2</sub> capture performance of MgO based sorbents. The use of alkali metal nitrates exploits the fact that they melt during the CO<sub>2</sub> capture process. The molten nitrate prevents the formation a solid MgCO<sub>3</sub> layer on the surface of MgO. Fig. 7 illustrates the function of the molten nitrate to promote the carbonation of MgO. The most commonly used nitrate promoters are NaNO<sub>3</sub> and KNO<sub>3</sub>. Because these nitrates do not directly react with CO<sub>2</sub>, the CO<sub>2</sub>



Fig. 7 The role of the MgO sorbent with nitrate salts for improving CO<sub>2</sub> capture capacity.



capture capacity is governed by the amount of active MgO available in the solid.<sup>83</sup> In addition to alkali metal nitrates, alkali metal carbonates could also enhance the performance of MgO sorbents, rendering both faster kinetics and higher uptake capacity. Further enhancements can be achieved when carbonate and nitrate promoters are used concomitantly. These different approaches to promote MgO sorbents are discussed below.

**3.1.1 Sodium nitrate (NaNO<sub>3</sub>).** The simple use of NaNO<sub>3</sub> as a promoter for MgO sorbent has been explored by a number of researchers. Studies using NaNO<sub>3</sub> as the only promoter have demonstrated effective promotional effects, reporting that doping ~7–11 mol% NaNO<sub>3</sub> by impregnation is the most effective in enhancing CO<sub>2</sub> uptake by MgO, despite the variabilities in CO<sub>2</sub> uptake report by different studies; the variabilities are likely to be results of the different synthesis procedures used.<sup>52,84,85</sup> Zhao *et al.*<sup>84</sup> studied calcined mesoporous MgO, synthesised by hydrothermal process (using Mg(CH<sub>3</sub>COO)<sub>2</sub> and urea), and reported the highest CO<sub>2</sub> uptake of 66.90 wt% (61.3 mol%) on MgO promoted with 7 mol% of NaNO<sub>3</sub>; this is over 40 times the CO<sub>2</sub> uptake by pure MgO 1.28 wt% (1.2 mol%). The promotional effect was associated with the formation of triple phase boundaries between the MgO, the promoters and the gas phase.<sup>84</sup> With too little NaNO<sub>3</sub>, the reaction at the phase boundaries and at the outer layer of the carbonate would be limited. In contrast, too much NaNO<sub>3</sub> would reduce the solubility of CO<sub>2</sub> as well as the contact between MgO and CO<sub>2</sub>, thus limiting the CO<sub>2</sub> capture capacity.<sup>84</sup>

**3.1.2 Mixed metal nitrates.** Mixed metal nitrates can also be used to create analogous promotional effects. Harada *et al.*<sup>86</sup> showed that 15 mol% (Li–Na–K)NO<sub>3</sub> on colloidal MgO nanoclusters prepared by sol–gel exhibited a high CO<sub>2</sub> uptake capacity of 69.10 wt% (63.3 mol%) at 340 °C. Dal Pozzo *et al.*<sup>85</sup> obtained promoted MgO by wet mixing commercial MgCO<sub>3</sub> with metal salts, followed by calcination at 450 °C. They showed that (Li, Na)NO<sub>3</sub>, (Li, K)NO<sub>3</sub> and (Li, Na, K)NO<sub>3</sub> all promoted MgO sorbents in a similar manner to when NaNO<sub>3</sub> was the only promoter, reporting CO<sub>2</sub> uptake ~38–43 wt% (35–39 mol%). Additionally, the MgO promoted by (Li, Na, K)NO<sub>3</sub> showed relatively stable performance over 10 cycles.

**3.1.3 Nitrites.** The use of nitrites can be an alternative or complement to nitrate promoters. In addition to using nitrates, Harada *et al.*<sup>86</sup> promoted colloidal MgO nanoclusters with LiNO<sub>3</sub>–(Na–K)NO<sub>2</sub>. The nitrite-promoted MgO sorbent had a CO<sub>2</sub> uptake of 68.2 wt% (62.4 mol%) at 340 °C, with better cyclic stability than the MgO promoted by (Li–Na–K)NO<sub>3</sub> (Fig. 8). Zhao *et al.*<sup>84</sup> showed that using a mixture of nitrate and nitrite promoters can further enhance the performance of the hydrothermally synthesised MgO sorbents.<sup>84</sup> When 0–8 mol% NaNO<sub>2</sub> was doped to NaNO<sub>3</sub>-promoted MgO (with molar ratio of MgO : NaNO<sub>3</sub> = 1 : 0.07) the CO<sub>2</sub> uptake increased from 66.9 wt% (61.3 mol%) to over 87 wt% (80 mol%), whilst showing stable performance over 15 cycles.

**3.1.4 Carbonates.** The presence of a carbonate promoter facilitate easier melting and faster CO<sub>2</sub> transport through the carbonate layer. Kwak *et al.*<sup>87</sup> employed a triple eutectic alkali carbonate (TEC) design, in which the MgO sorbent was

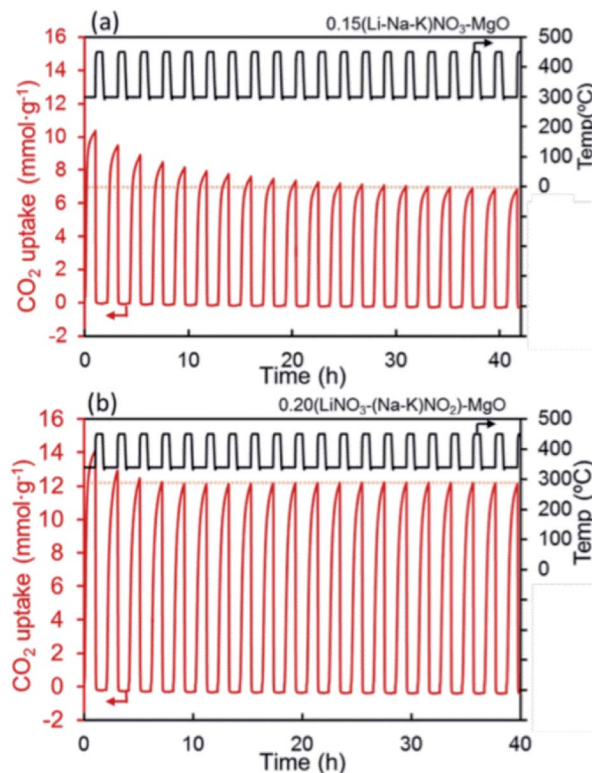


Fig. 8 CO<sub>2</sub> capture capacity of promoted MgO by alkali metal nitrates ((Li–Na–K)NO<sub>3</sub>) and nitrate/nitrite (LiNO<sub>3</sub>–(Na–K)NO<sub>2</sub>) salt. Reprinted with permission<sup>86</sup> copyright 2021 American Chemical Society.

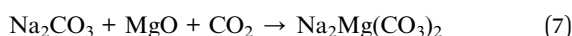
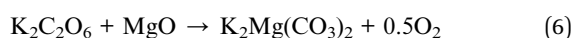
promoted by a TEC mixture consisting of Li<sub>2</sub>CO<sub>3</sub>, Na<sub>2</sub>CO<sub>3</sub>, and K<sub>2</sub>CO<sub>3</sub> (with a molar ratio of Li : Na : K of 0.435 : 0.315 : 0.250). They classified the CO<sub>2</sub> capture process into two steps: (1) “fast and large”, and (2) “slow and small”. The amount of TEC used affects the kinetics of these two steps differently – the rate of step 1 increases with increasing amount of TEC; but this was not observed for step 2. The optimal TEC amount was found to be 60 mol% (sample 60-TEC/MgO), which gave a CO<sub>2</sub> uptake of 43.4 wt% (39.7 mol%) in step 1 and an additional 33.9 wt% (31.0 mol%) in step 2. It was also found that MgO with low TEC content (20–40 mol%) had better cyclic stability than those with high TEC content (60–100 mol%).

**3.1.5 Carbonates with nitrite or nitrate.** Co-Doping of carbonates and nitrates has been a popular approach for developing promoted MgO based sorbents,<sup>83,88–91</sup> with key studies summarised in Table 3. Here, we discuss key synthetic parameters governing the performance of the co-doped sorbents. Hwang *et al.*<sup>83</sup> investigated the doping of K<sub>2</sub>CO<sub>3</sub> to NaNO<sub>3</sub> and KNO<sub>3</sub>-promoted commercial MgO and found the K<sub>2</sub>CO<sub>3</sub> : nitrate ratio to be important. Co-doping 30 wt% K<sub>2</sub>CO<sub>3</sub> with 10 wt% of NaNO<sub>3</sub> or KNO<sub>3</sub> both worked well, rendering 44 wt% (40 mol%) uptake at 300 °C in 20 atm CO<sub>2</sub>.<sup>83</sup> Vu *et al.*<sup>91</sup> promoted the performance of mesoporous MgO aerogels with double sodium salts (MgO·Na<sub>2</sub>CO<sub>3</sub>·NaNO<sub>3</sub>). During operation, Na<sub>2</sub>CO<sub>3</sub> and NaNO<sub>3</sub> facilitate a high concentration of O<sup>2–</sup> in the molten salts, which would enhance the CO<sub>2</sub> capture capacity by accelerating the formation of MgCO<sub>3</sub>. Furthermore, the molten salts hinder the





formation of the rate-limiting carbonate surface layers, whilst accelerating the production of  $\text{CO}_3^{2-}$ . Therefore, it is important to dope MgO with an optimal amount of alkali salts to maximise the benefit of eutectic formation. Specifically, the amount of  $\text{Na}_2\text{CO}_3$  should be equal to or less than the amount of  $\text{NaNO}_3$  for optimal  $\text{CO}_2$  capture performance. According to Vu *et al.*, the highest  $\text{CO}_2$  uptake of 56 wt% (51 mol%) was achieved at 325 °C (1 atm, pure  $\text{CO}_2$ ) when the molar ratio of  $\text{MgO} : \text{Na}_2\text{CO}_3 : \text{NaNO}_3$  was 1 : 0.05 : 0.2.<sup>91</sup> Wang *et al.*<sup>92</sup> also showed the benefit of having both nitrate and carbonate doped on MgO nano-sheets through a series of experiments and found that the optimal sorbent composition to be  $[(\text{LiNO}_3, \text{KNO}_3)_2(\text{Na}_2\text{CO}_3, \text{K}_2\text{CO}_3)]_{0.15}/\text{MgO}$ , which showed a high  $\text{CO}_2$  uptake of 73 wt% (67 mol%) (350 °C, 1 atm, 100%  $\text{CO}_2$ ). They proposed a reaction mechanism between  $\text{CO}_2$  and the sorbent, involving the following steps:



The finding of Wang *et al.*<sup>92</sup> was in agreement with Ding *et al.*,<sup>88</sup> who revealed that the reaction between  $\text{CO}_2$  and MgO promoted with 10 mol%  $[(\text{Li}_{0.44}\text{K}_{0.56})\text{NO}_3]_2[(\text{Na}_{0.5}\text{K}_{0.5})\text{CO}_3]$  takes place in three stages: (1) the formation of carbonate in the first 7 minutes – at this stage,  $\text{CO}_2$  is dissolved in the molten salt and then reacts with MgO and formed a layer of carbonate ( $\text{CO}_3^{2-}$ ), producing  $\text{K}_2\text{C}_2\text{O}_6$  and  $\text{K}_2\text{Mg}(\text{CO}_3)_2$ . (2) The restriction of the rigid carbonate layer and the formation of the high concentration of oxygen ion within 10 minutes – oxygen ions ( $\text{O}^{2-}$ ) are produced by the dissolution of MgO and the decomposition of the molten alkali nitrates and nitrites. (3) The nucleation of magnesium carbonate occurs between 10 and 60 minutes after contacting the  $\text{CO}_2$ .

### 3.2 Structured MgO sorbents

Morphological features, such as surface area, pore volume, size and thickness of the particle are all critical to the performance of MgO sorbents.<sup>93</sup> Therefore, researchers have explored various synthetic approaches to improve the morphological properties of MgO sorbents to enhance their  $\text{CO}_2$  uptake.<sup>94–96</sup> In general, the  $\text{CO}_2$  uptake correlates well to the sorbent's surface area. Guo *et al.*<sup>94</sup> showed that solid state chemical reaction (SR) method produced MgO with, smaller particle sizes, higher BET surface area ( $100 \text{ m}^2 \text{ g}^{-1}$ ), smaller pore sizes and higher pore volume ( $0.67 \text{ cm}^3 \text{ g}^{-1}$ ) than those produced by other synthesis methods, such as direct calcination (DC), direct precipitation (DP) and sol-gel (SG) – when  $\text{MgCl}_2$  was used as the Mg precursor in all the synthesis methods. As a result, MgO synthesised by SR showed higher  $\text{CO}_2$  uptake (10.5 wt%, 9.6 mol%) than those by the DC, DP and SG methods, which yielded  $\text{CO}_2$  uptakes of 2.95–6.8 wt% (2.7–6.2 mol%). In addition, the  $\text{CO}_2$  capture capacities are also correlated to the sorbents' basicity, which are classified as weak, medium and strong. Accordingly, the SR method yielded the highest number of medium and strong basic sites (responsible for 2.54 and 1.24 mmol  $\text{CO}_2$  per g of uptake, respectively) as well

as the highest total amount of basic sites (with a total uptake of 5.49 mmol  $\text{CO}_2$  per g). The abundant basic sites enhanced the  $\text{CO}_2$  uptake of the SR sorbent. Similarly, Ding *et al.*<sup>95</sup> showed that MgO synthesised from magnesium acetate tetrahydrate ( $\text{Mg}(\text{CH}_3\text{COO})_2$ ) and oxalic acid ( $\text{C}_2\text{H}_2\text{O}_4$ ) dihydrate solution (MgO–MO) had a high BET surface area of  $252 \text{ m}^2 \text{ g}^{-1}$ , high pore volume of  $0.763 \text{ cm}^3 \text{ g}^{-1}$  and  $\text{CO}_2$  uptake capacity of 7.59 wt% (7.0 mol%) at 50 °C. The  $\text{CO}_2$  uptake capacity of MgO–MO was superior compared to MgO synthesised by calcining magnesium carbonate (MgO–BMC), the rehydration of MgO–BMC (MgO–RF) and commercial MgO (MgO–CA).<sup>95</sup> Hanif *et al.*<sup>96</sup> found that MgO obtained by ammonia precipitation (AC) showed higher surface area ( $362 \text{ m}^2 \text{ g}^{-1}$ ,  $0.701 \text{ cm}^3 \text{ g}^{-1}$ ) and  $\text{CO}_2$  uptake 7.53 wt% (6.9 mol%) than those by urea hydrolysis (UC) and thermal degradation (TC).

Researchers have also developed porous MgO with structural regularities as a means to control the morphologies of the synthetic sorbents. The performance of the various MgO sorbents with well-defined morphologies is summarised in Fig. 9. Notable morphologies are discussed in details below (Fig. 10).

**3.2.1 Sheets.** Wang *et al.*<sup>92</sup> synthesised sheet-like  $[(\text{Li}, \text{K})_2(\text{Na}, \text{K})]_{0.15}/\text{MgO}$  having a sheet thickness of  $\sim 40 \text{ nm}$ . The MgO nanosheets showed higher  $\text{CO}_2$  uptake than granular MgO because the former had more surface MgO, which can readily react with  $\text{CO}_2$ . This advantage is corroborated by the nanosheets' larger BET surface area ( $56 \text{ m}^2 \text{ g}^{-1}$ ), larger pore volume ( $0.24 \text{ cm}^3 \text{ g}^{-1}$ ) and larger mean pore diameter than the granular MgO. Additionally, the sheet-like MgO sorbents showed relatively stable performance over 20 cycles.  $\text{CO}_2$  uptake capacity is summarised by the morphology with the surface area in Fig. 9.

**3.2.2 Platelets.** Hanif *et al.*<sup>96</sup> prepared both platelet, sheet-like and octahedra structured MgO sorbents. They found that platelet morphology shows larger BET surface area ( $362 \text{ m}^2 \text{ g}^{-1}$ ), higher pore volume ( $0.701 \text{ cm}^3 \text{ g}^{-1}$ ) and relatively higher  $\text{CO}_2$  uptake of 7.53 wt% (6.9 mol%) than the other two morphologies.

**3.2.3 Rods.** Zhao *et al.*<sup>84</sup> and Tuan *et al.*<sup>97</sup> found rod-like MgO to perform better than other tested shapes such as MgO spheres (they are described as 'ball-like' in the original paper).

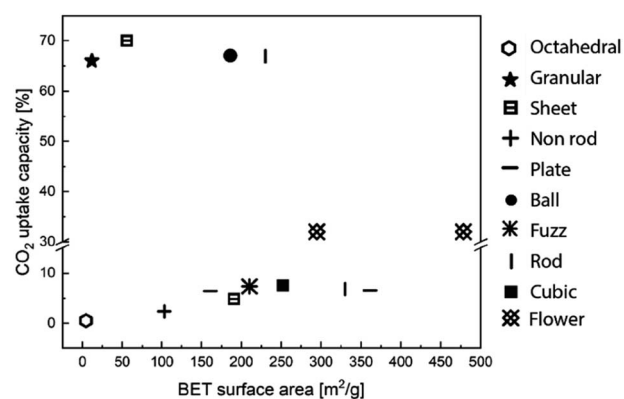


Fig. 9  $\text{CO}_2$  uptake capacity and BET surface area according to the various structure of MgO sorbents. The data points entries are obtained from ref. 84, 92, 95, 96, 98 and 99.



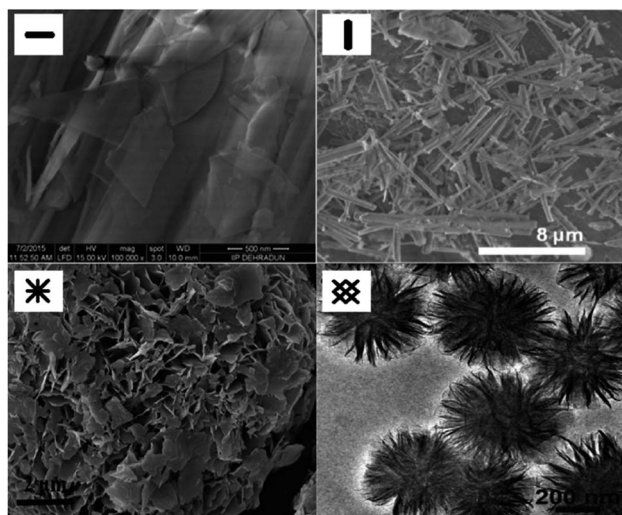


Fig. 10 SEM images of the structure of MgO sorbents: plate,<sup>96</sup> rod,<sup>97</sup> and fuzz-like structure of MgO sorbents<sup>95</sup> and TEM image of the flower-like plate,<sup>98</sup> Reprinted with permission copyright 2021 American Chemical Society.<sup>96</sup> Reprinted with permission copyright 2021 Royal Society of Chemistry,<sup>95</sup> Reprinted with permission copyright 2021 John Wiley and Son, Inc.<sup>97,98</sup>

Both teams attributed the enhanced CO<sub>2</sub> uptake by the rod-like MgO to their high BET surface area (230–331 m<sup>2</sup> g<sup>-1</sup>), larger pore volume (0.49–0.58 cm<sup>3</sup> g<sup>-1</sup>) as well as small particle sizes (~7 nm in both studies). CO<sub>2</sub> uptake capacity of rod-like MgO are drawn in Fig. 9.

**3.2.4 Cubes.** Cubic morphology may not be a trivial morphology that is typically associated with high specific surface areas. However, Ding *et al.*<sup>95</sup> reported a sorbent consisting of cube-like MgO grains with high BET surface area and pore volume (252 m<sup>2</sup> g<sup>-1</sup>, 0.76 cm<sup>3</sup> g<sup>-1</sup>). The MgO microcubes showed a CO<sub>2</sub> uptake capacity of 7.59 wt% (7.0 mol%), outperforming the plate-like MgO 6.44 wt% (5.9 mol%) prepared in the same study. Both of CO<sub>2</sub> uptake capacity are added in Fig. 9.

**3.2.5 Flower.** Li *et al.*<sup>98,99</sup> synthesised MgO/C composites with flower-like morphology. The large surface area and pore volume (295 m<sup>2</sup> g<sup>-1</sup>, 0.94 cm<sup>3</sup> g<sup>-1</sup>)<sup>98</sup> of the flower-like morphology facilitated efficient mass transport and improved the CO<sub>2</sub> uptake capacity of the MgO sorbents. Experimentally, the MgO/C nanocomposite showed a high CO<sub>2</sub> uptake of 30.9 wt% (28.3 mol%) at 27 °C, 1 bar. Using a similar synthetic strategy, Li *et al.*<sup>100</sup> combined the flowerlike MgO/C with the sheet-like graphene oxide and produced a sandwich-like structure with surface area (478 m<sup>2</sup> g<sup>-1</sup>) and pore volume (1.22 cm<sup>3</sup> g<sup>-1</sup>) even higher than the graphene oxide-free MgO/C nanocomposite. The sandwich-like structured showed an apparent uptake capacity of 31.5 wt% (28.8 mol%),<sup>100</sup> also plotted in Fig. 9.

### 3.3 Summary and knowledge gap

MgO based materials are promising CO<sub>2</sub> sorbents for applications at moderately high temperatures. When low-grade heat (<400 °C) is abundantly available on-site, using MgO to capture CO<sub>2</sub> may be more advantageous than calcium looping.<sup>101</sup> Additionally, MgO has the potential to become a highly effective CO<sub>2</sub>

sorbent if its stoichiometric capture capacity can be fully exploited. In practice, the performance of MgO based sorbents is significantly hindered by its unfavourable carbonation mechanism and sluggish rates. Many different approaches have been studied to promote the uptake of CO<sub>2</sub> by MgO. Whilst high surface area, morphologically well-defined MgO sorbents could significantly improve CO<sub>2</sub> uptake, the experimentally accessible capacities are still substantially lower than the CaO based sorbents. Also, carbonation–calcination cycles could induce drastic morphological changes to the sorbents, making the morphologies of the freshly-prepared materials less relevant to the long-term performance.<sup>102</sup> Alternatively, the doping of alkaline metal salts to form low-melting eutectics is a much more effective to tackle the issue of the slow CO<sub>2</sub> uptake kinetics. However, the underlying science governing the promotional effects, including the interaction between the different salts in the eutectics, the interplay between different phases (*e.g.* molten salt, MgO and MgCO<sub>3</sub>) and the mechanisms of ionic diffusion in the molten salt, must be further studied and better understood.<sup>103</sup> Lastly, many MgO sorbents suffer from poor cyclic stability. Therefore, further development is required to improve the effectiveness of the MgO based sorbents.

## 4 Li, Na, K, Sr and Ba based sorbents

As briefly discussed in Section 1, the carbonation of Li<sub>2</sub>O, Na<sub>2</sub>O, K<sub>2</sub>O, SrO and BaO is practically irreversible. However, irreversible CO<sub>2</sub> sorbents are economically unattractive as they cannot be recycled and reused in continuous processes. Therefore, Li, Na, K, Sr and Ba based sorbents are often formulated as ternary oxides consisting of (i) at least one alkali metal or alkaline earth metal and (ii) at least one transition metal or semi-metal. The presence of transition metals and semi-metals introduces acidity to the ternary oxides and modulates the overall basicity of the sorbents, making them thermally regenerable at practically achievable temperatures. This section discusses the recent

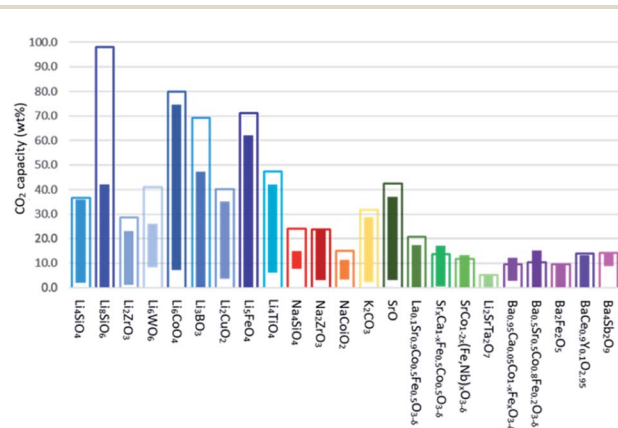


Fig. 11 Theoretical and experimental CO<sub>2</sub> uptake capacities of various Li-, Na-, K-, Sr- and Ba- based CO<sub>2</sub> sorbents. The hollow bars represent the stoichiometric capture capacities, whereas the solid bars represent the range of experimentally measured CO<sub>2</sub> uptakes. The sorbents are classified according to the chemical composition of the active components, *i.e.* excluding the formulation of the support.





Table 4 Various reaction conditions and capacities of Li, Na, K, Sr and Ba based sorbents<sup>a</sup>

| Sorbent  | Synthesis method | BET [m <sup>2</sup> g <sup>-1</sup> ] | Stoichiometric CO <sub>2</sub> capacity [wt%] | Experimental CO <sub>2</sub> uptake |            | Carbonation temperature [°C] | Calcination temperature [°C] | Carbonation CO <sub>2</sub> partial pressure [bar] | Calcination CO <sub>2</sub> partial pressure [bar] | Max no. of cycles | Ref.            |
|--|------------------|---------------------------------------|---|-------------------------------------|------------|------------------------------|------------------------------|--|--|-------------------|-----------------|
|  |                  |                                       |   | [wt%]                               | [mol%]     |                              |                              |  |  |                   |                 |
| Li <sub>4</sub> SiO <sub>4</sub>   | a, b, c          | 0.06–10                               | 36.7  | 1.8–36.0                            | 4.9–98.1   | RT–700 <sup>b</sup>          | 550–900                      | 0.04–1.0   | 0  | 250               | 114 and 116–121 |
| Li <sub>8</sub> SiO <sub>6</sub>   | a                | —                                     | 98.0  | 0–42.0                              | 0–42.9     | 25–776 <sup>b</sup>          | —                            | 1.5  | —  | —                 | 115             |
| Li <sub>2</sub> ZrO <sub>3</sub>   | a, b, c          | 2–3                                   | 28.7  | 0.01–23.0                           | 0–80.1     | 500–575                      | 600–700                      | 0.10–2.0   | 0–0.585  | 30                | 122–124         |
| Li <sub>6</sub> WO <sub>6</sub>  | a                | 8                                     | 41.1  | 3.6–25.9                            | 8.8–63.0   | 30–710 <sup>b</sup>          | 730–760                      | 0.60   | 0  | 4                 | 130             |
| Li <sub>6</sub> CoO <sub>4</sub>   | a                | 1                                     | 80.0  | 5.0–76.4                            | 6.3–95.5   | 300–700                      | 700–750                      | 0.20–1.0   | 0  | 10                | 127             |
| Li <sub>3</sub> BO <sub>3</sub>  | c, d             | 1–3                                   | 69.1  | 0–47.2                              | 0–68.3     | 500–650                      | 650                          | 0.20–1.0   | 0  | 10                | 131             |
| Li <sub>2</sub> CuO <sub>2</sub>   | a, c             | 1–6                                   | 40.2  | 3.6–37.4                            | 9.0–93.0   | 30–750 <sup>b</sup>          | 750–850                      | 1.0–5.0  | 0  | —                 | 128 and 129     |
| Li <sub>5</sub> FeO <sub>4</sub>   | a                | —                                     | 71.2  | 0–62.0                              | 0–87.1     | 30–700 <sup>b</sup>          | —                            | 1.0  | —  | —                 | 126             |
| Li <sub>4</sub> TiO <sub>4</sub>   | a                | —                                     | 47.3  | 0–42.0                              | 0–88.8     | 300–856                      | —                            | 1.0  | —  | —                 | 125             |
| Na <sub>4</sub> SiO <sub>4</sub>   | d                | —                                     | 23.9  | 7.7–19.2                            | 32.2–80.3  | 50–840 <sup>b</sup>          | —                            | 0.80   | —  | —                 | 133             |
| Na <sub>2</sub> ZrO <sub>3</sub>   | a, d             | 4–5                                   | 23.8  | 4.5–23.8                            | 18.9–100.0 | 150–800                      | 680–900                      | 0.025–1.0  | 0  | 70                | 134–137         |
| NaCoO <sub>2</sub>   | a                | —                                     | 15.0  | 3.3–11.1                            | 22.0–73.3  | 100–800                      | —                            | 0.050–1.0  | —  | —                 | 132             |
| K <sub>2</sub> CO <sub>3</sub>   | b, c, e          | 0.4–459                               | 31.8  | 4.3–28.7                            | 13.5–90.3  | 50–100                       | 60–300                       | 0.010–0.18   | 0–1.0  | 10                | 138–143         |
| SrO  | e                | 1–3                                   | 42.5  | 3.0–37.1                            | 7.1–87.3   | 1100–1200                    | 1100–1200                    | 0.30–0.50  | 0  | 10                | 144             |
| Li <sub>0.1</sub> Sr <sub>0.5</sub> Co <sub>0.5</sub> Fe <sub>0.5</sub> O <sub>3–δ</sub> | f                | —                                     | 20.7  | 0–17.3                              | 0–83.6     | 600–800                      | —                            | 0.10–1.0   | —  | —                 | 145             |
| Sr <sub>x</sub> Ca <sub>1–x</sub> Fe <sub>0.5</sub> Co <sub>0.5</sub> O <sub>3–δ</sub>   | f                | —                                     | 27.3  | 0.4–17.0                            | 1.5–62.3   | RT–950 <sup>b</sup>          | —                            | 1.0  | —  | —                 | 146–148         |
| SrCo <sub>1–2x</sub> (Fe, Nb) <sub>x</sub> O <sub>3–δ</sub>                              | a                | —                                     | 23.6  | 0–13.1                              | 0–55.5     | 925                          | —                            | 0.75   | —  | —                 | 149             |
| Li <sub>2</sub> SrTa <sub>2</sub> O <sub>7</sub>   | —                | —                                     | 5.1   | 0–4.9                               | 0–96.1     | 140                          | 700                          | —  | —  | 6                 | 151             |
| Ba <sub>0.95</sub> Ca <sub>0.05</sub> Co <sub>1–x</sub> Fe <sub>x</sub> O <sub>3–δ</sub> | f                | —                                     | 19.2  | 2.8–12.0                            | 14.6–62.5  | 850                          | —                            | 0.10   | —  | —                 | 148             |
| Ba <sub>0.5</sub> Sr <sub>0.5</sub> Co <sub>0.5</sub> Fe <sub>0.2</sub> O <sub>3–δ</sub> | a                | —                                     | 20.9  | 0–14.9                              | 0–71.4     | RT–950 <sup>b</sup>          | —                            | 1.0  | —  | —                 | 149             |
| Ba <sub>2</sub> Fe <sub>2</sub> O <sub>5</sub>   | a                | —                                     | 18.8  | 0–9.4                               | 0–50.0     | 1000                         | 1000                         | 1.0  | 0  | —                 | 153 and 154     |
| BaCe <sub>0.9</sub> Y <sub>0.1</sub> O <sub>2.95</sub>                                   | a                | —                                     | 13.8  | 0–13.1                              | 0–94.9     | 600–1000                     | —                            | 1.0  | —  | —                 | 152             |
| Ba <sub>4</sub> Sb <sub>2</sub> O <sub>9</sub>   | a                | —                                     | 14.1  | 9.5–14.0                            | 67.4–99.3  | 650–750                      | 950                          | 0.42   | 1  | 100               | 155             |

<sup>a</sup> Synthesis methods: (a) solid state; (b) impregnation suspension; (c) doping; (d) wet chemistry; (e) calcination; (f) citrate sol–gel method. <sup>b</sup> Indicates temperature programmed CO<sub>2</sub> capture experiments in a TGA.



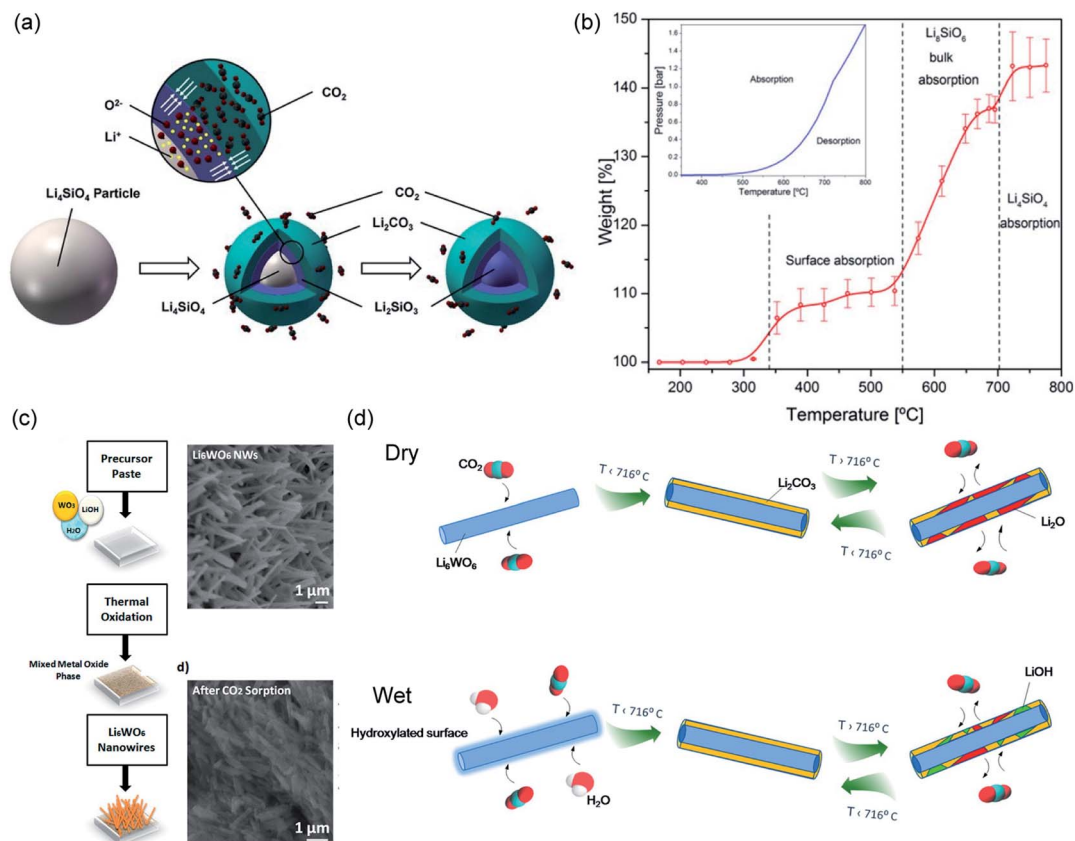


Fig. 12 (a) Schematic illustration of the "double shell" model describing  $\text{Li}_4\text{SiO}_4$  carbonation. Reprinted with permission<sup>114</sup> copyright 2021 John Wiley and Son, Inc. (b) Temperature-programmed carbonation of  $\text{Li}_8\text{SiO}_6$  in a TGA. Reprinted with permission<sup>115</sup> copyright 2021 American Chemical Society. (c) Illustration of synthesis of  $\text{Li}_6\text{WO}_6$  NWs and its morphological change 30 min of carbonation at 700 °C. Reprinted with permission<sup>91</sup> copyright 2021 American Chemical Society. (d) Schematic illustration of  $\text{CO}_2$  capture and release on  $\text{Li}_6\text{WO}_6$  NWs under dry and wet conditions. Reprinted with permission<sup>1</sup> copyright 2021 American Chemical Society.

development in the formulation, synthesis and the  $\text{CO}_2$  capture performance of synthetic Li, Na, K, Sr and Ba based sorbents. Fig. 11 summarises the stoichiometric and experimental  $\text{CO}_2$  uptake capacities of the Li, Na, K, Sr and Ba based sorbents reported in the recent literature. A more elaborated summary is provided in Table 4.

#### 4.1 Li based sorbents

**4.1.1 Lithium silicates.** Lithium silicates, including  $\text{Li}_4\text{SiO}_4$  and  $\text{Li}_8\text{SiO}_6$ , are considered to be the most studied lithium based sorbents. The carbonation mechanism of these ternary oxides are fundamentally different from the CaO and MgO based ones, as more than one solid phases will form during carbonation.  $\text{Li}_4\text{SiO}_4$  reacts with  $\text{CO}_2$  between 450 and 700 °C with a stoichiometric  $\text{CO}_2$  uptake capacity of 36.7 wt% according to:



The two solid products arrange themselves following a double-shell model, in which  $\text{Li}_2\text{CO}_3$  and  $\text{Li}_2\text{SiO}_3$  form an outer shell and an inner shell, respectively, as depicted in Fig. 12a.<sup>114</sup> The inner  $\text{Li}_2\text{SiO}_3$  shell encapsulates the unreacted  $\text{Li}_4\text{SiO}_4$  core. Once the shells have fully developed, further

carbonation requires the migration of  $\text{CO}_2$  inward through the  $\text{Li}_2\text{CO}_3$  layer, and the migration of  $\text{Li}^+$  and  $\text{O}_2^-$  ions outward through the  $\text{Li}_2\text{SiO}_3$  layer. Therefore, the interface between  $\text{Li}_2\text{CO}_3$  and  $\text{Li}_2\text{SiO}_3$  is regarded as the reaction front, where new  $\text{Li}_2\text{CO}_3$  forms. As both shells grow thicker, the diffusion resistance increases and slows down the rate. It is believed that the diffusion of  $\text{CO}_2$  through the  $\text{Li}_2\text{CO}_3$  layer is the rate limiting step, because the diffusion of  $\text{CO}_2$  through the carbonate is considered slower than the diffusion of  $\text{Li}^+$  and  $\text{O}_2^-$  through the silicate. Owing to the product layer diffusion resistances, the experimentally accessible uptake capacities are always lower than the stoichiometric values. For the chemically unmodified lithium silicates, the surface area of the sorbent becomes the effective rate limiting factor, which subsequently determines the practically achievable uptake capacity.

Using a lithium-rich compound such as  $\text{Li}_8\text{SiO}_6$  could potentially improve the  $\text{CO}_2$  uptake to 98 wt%. The carbonation of  $\text{Li}_8\text{SiO}_6$  consists of 3 steps, as illustrated in Fig. 12b and confirmed by *in situ* synchrotron powder X-ray diffraction (SPXRD):<sup>115</sup>

Steps 1 and 2 involve the uptake of  $\text{CO}_2$  by  $\text{Li}_8\text{SiO}_6$  on the surface and in the bulk:



Step 3 involves the uptake of CO<sub>2</sub> by the formed Li<sub>4</sub>SiO<sub>4</sub>:



Lithium silicates can be easily synthesised by solid-state reactions. A typical synthesis involves mechanically mixing lithium and silicon precursors with desired stoichiometric ratios, followed by drying and calcination (at 800–900 °C). Typical lithium precursors include Li<sub>2</sub>CO<sub>3</sub>,<sup>116,117</sup> Li<sub>2</sub>O (ref. 118) and LiNO<sub>3</sub>,<sup>119</sup> whereas the silicon precursor is almost always SiO<sub>2</sub>. Regardless of the precursor used, solid-state synthesised lithium silicates exhibit low specific surface areas (<1 m<sup>2</sup> g<sup>-1</sup>) and low experimental CO<sub>2</sub> uptake capacities: 28–35 wt% (76–95 mol%) for Li<sub>4</sub>SiO<sub>4</sub> (ref. 116 and 117) and 42 wt% (43 mol%) for Li<sub>8</sub>SiO<sub>6</sub>.<sup>115</sup> In addition, the poor sintering resistance of the solid product, Li<sub>2</sub>SiO<sub>3</sub>, results in rapid performance decay over CO<sub>2</sub> capture cycles.<sup>117</sup>

Given the dependence on product layer diffusion during carbonation, it is intuitive to prepare Li<sub>4</sub>SiO<sub>4</sub> sorbents with high surface areas using wet chemistry methods such as impregnation suspension,<sup>114,120</sup> which involves mixing an aqueous solution of lithium precursors (*e.g.* lithium acetate and lithium lactate) with a SiO<sub>2</sub> sol suspension, which is subsequently dried and calcined.<sup>114</sup> Indeed, the resulting Li<sub>4</sub>SiO<sub>4</sub> samples exhibit higher surface areas (1.6–2 m<sup>2</sup> g<sup>-1</sup>), higher CO<sub>2</sub> uptake (up to 36 wt%, *i.e.* 98 mol%) and better cyclic durability (over 40 cycles) than those synthesised by solid-state reactions.<sup>114</sup>

Alternatively, the performance of Li<sub>4</sub>SiO<sub>4</sub> can be improved by doping. Inert dopants (*e.g.* CaCO<sub>3</sub>) can increase the sorbents' specific surface area and sintering resistance.<sup>117</sup> Low melting-point dopants, *e.g.* Na<sub>2</sub>CO<sub>3</sub>, K<sub>2</sub>CO<sub>3</sub>, NaNO<sub>3</sub> and KNO<sub>3</sub>, can accelerate the transport of CO<sub>2</sub> through the Li<sub>2</sub>CO<sub>3</sub> product layer, analogous to the case of alkali metal salt doped MgO sorbents.<sup>119–121</sup> Lastly, redox-active dopants, such as Fe<sup>3+</sup>, can improve the transport of O<sup>2-</sup> ions through the Li<sub>2</sub>SiO<sub>3</sub> product layer.<sup>118</sup> Synthetically, doping can be achieved by including dopant precursors during the solid state synthesis of the Li<sub>4</sub>SiO<sub>4</sub> sorbent,<sup>116,117</sup> impregnating the solid-state synthesised Li<sub>4</sub>SiO<sub>4</sub> with soluble dopants (*e.g.* Na<sub>2</sub>CO<sub>3</sub>, K<sub>2</sub>CO<sub>3</sub>, NaNO<sub>3</sub> and KNO<sub>3</sub>), or performing a secondary solid state reaction between the as-synthesised Li<sub>4</sub>SiO<sub>4</sub> and the dopant precursor. Two-step solid state synthesis was used for the synthesis of Li<sub>4+x</sub>Si<sub>1-x</sub>Fe<sub>x</sub>O<sub>4</sub> sorbents from Li<sub>4</sub>SiO<sub>4</sub> and Li<sub>3</sub>FeO<sub>4</sub>.<sup>118</sup> As an economic and sustainable alternative, Wang *et al.* used acid-leached blast

furnace slag, which contains TiO<sub>2</sub>, Fe<sub>2</sub>O<sub>3</sub>, Al<sub>2</sub>O<sub>3</sub>, CaO and K<sub>2</sub>O, as the silicon precursor for the solid-state synthesis of Li<sub>4</sub>SiO<sub>4</sub>.<sup>116</sup> The inherent presence of dopants in the silica precursor offers a cost-effective means to prepare high performance Li<sub>4</sub>SiO<sub>4</sub> sorbents. In all cases, the dopant-promoted Li<sub>4</sub>SiO<sub>4</sub> showed increased specific surface area (from 0.06 to 0.3 m<sup>2</sup> g<sup>-1</sup>), improved CO<sub>2</sub> uptake (up to 35 wt%, *i.e.* 95 mol%),<sup>117</sup> improved cyclic stability (up to 250 cycles)<sup>121</sup> and faster rate of carbonation at low reaction temperatures in low CO<sub>2</sub> concentrations (in 20% CO<sub>2</sub> at 200 °C).<sup>118</sup>

**4.1.2 Other Li based sorbents.** Lithium zirconate (Li<sub>2</sub>ZrO<sub>3</sub>) is the second most studied lithium based sorbent with a stoichiometric uptake capacity of 28.7 wt%:



The experimentally reported carbonation temperatures are in the range of 450–650 °C. Similar to lithium silicates, the carbonation of Li<sub>2</sub>ZrO<sub>3</sub> also proceeds *via* a double shell model, in which the inner and outer product layers are ZrO<sub>2</sub> and Li<sub>2</sub>CO<sub>3</sub>, respectively. The CO<sub>2</sub> diffusion through the Li<sub>2</sub>CO<sub>3</sub> inner layer is considered to be the rate limiting step. Li<sub>2</sub>ZrO<sub>3</sub> can be simply synthesised by solid-state reaction from Li<sub>2</sub>CO<sub>3</sub> and ZrO<sub>2</sub>. However, solid-state synthesised Li<sub>2</sub>ZrO<sub>3</sub> show slow carbonation and low uptake capacities (5.9–10 wt%, *i.e.* 20.6–34.8 mol%).<sup>122,123</sup> Therefore, synthetic methods used to improve the performance of Li<sub>4</sub>SiO<sub>4</sub> have also been adopted to promote the Li<sub>2</sub>ZrO<sub>3</sub> sorbents, such as (i) doping low-melting point salts to improve the CO<sub>2</sub> mobility through the carbonate product layer,<sup>123</sup> (ii) doping redox-active Fe<sup>3+</sup> to improve the O<sub>2</sub><sup>-</sup>-CO<sub>3</sub><sup>2-</sup> bi-ionic diffusivity through the Li<sub>2</sub>CO<sub>3</sub> product layer,<sup>122</sup> and (iii) preparing Li<sub>2</sub>ZrO<sub>3</sub>-Na<sub>2</sub>ZrO<sub>3</sub> solid-solution sorbents by impregnation suspension.<sup>124</sup> Methods (i) and (iii) appear to be more effective in enhancing CO<sub>2</sub> uptake (20–22 wt%, *i.e.* 70–77 mol%), whereas the improvement by Fe-doping is marginal (7.0–9.2 wt%, *i.e.* 24.4–32.1 mol%).

Ternary oxide phases containing Li and transition metals have also been prepared, primarily by solid-state synthesis, as CO<sub>2</sub> sorbents.<sup>125–130</sup> A summary of the carbonation chemistries of these Li-transition metal oxides is presented in Table 5. Amongst these ternary oxides, Li<sub>6</sub>CoO<sub>4</sub> has both the highest stoichiometric CO<sub>2</sub> uptake and the highest experimental CO<sub>2</sub> uptake of 80.0 and 74.5 wt%, respectively,<sup>127</sup> whereas Li<sub>6</sub>WO<sub>6</sub> nanowires showed the ability to rapidly capture CO<sub>2</sub> at ambient

Table 5 Summary of carbonation reactions of Li-transition metal-oxide materials

| Active sorbent                   | Carbonation reactions   | Stoichiometric CO <sub>2</sub> uptake capacity (wt%) |
|----------------------------------|---|--|
| Li <sub>4</sub> TiO <sub>4</sub> | Li <sub>4</sub> TiO <sub>4</sub> + 4CO <sub>2</sub> = 4Li <sub>2</sub> CO <sub>3</sub> + TiO <sub>2</sub>             | 41.5–47.3  |
| Li <sub>3</sub> FeO <sub>4</sub> | Li <sub>3</sub> FeO <sub>4</sub> + 2CO <sub>2</sub> = LiFeO <sub>2</sub> + 2Li <sub>2</sub> CO <sub>3</sub>           | 71.2   |
|                                  | LiFeO <sub>2</sub> + CO <sub>2</sub> = Li <sub>2</sub> CO <sub>3</sub> + Fe <sub>2</sub> O <sub>3</sub>               |  |
| Li <sub>6</sub> CoO <sub>4</sub> | Li <sub>6</sub> CoO <sub>4</sub> + 3CO <sub>2</sub> = 3Li <sub>2</sub> CO <sub>3</sub> + CoO                          | 80   |
| Li <sub>2</sub> CuO <sub>2</sub> | Li <sub>2</sub> CuO <sub>2</sub> + CO <sub>2</sub> = Li <sub>2</sub> CO <sub>3</sub> + CuO                            | 40.2   |
| Li <sub>6</sub> WO <sub>6</sub>  | Li <sub>6</sub> WO <sub>6</sub> + CO <sub>2</sub> = Li <sub>4</sub> WO <sub>5</sub> + Li <sub>2</sub> CO <sub>3</sub> | 41.1   |
|                                  | Li <sub>4</sub> WO <sub>5</sub> + CO <sub>2</sub> = Li <sub>2</sub> WO <sub>4</sub> + Li <sub>2</sub> CO <sub>3</sub> |  |
|                                  | Li <sub>2</sub> WO <sub>4</sub> + CO <sub>2</sub> = WO <sub>3</sub> + Li <sub>2</sub> CO <sub>3</sub>                 |  |



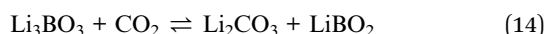
temperatures in the presence of moisture (relative humidity =  $58 \pm 3\%$ ). The high performance of  $\text{Li}_6\text{WO}_6$  nanowires at ambient temperatures is attributed to the hydration and activation of the surface of the nanowires for accelerated carbonation, as illustrated in Fig. 12d.<sup>127</sup> For sorbents containing redox-active metals, *e.g.* Co and Fe, the redox environment during carbonation will also affect the  $\text{CO}_2$  capture performance. For instance, the presence of  $\text{O}_2$  promotes  $\text{CO}_2$  uptake of  $\text{Li}_5\text{FeO}_4$  by enhancing the ionic diffusion through the product layer.<sup>118</sup> In contrast, the performance of  $\text{Li}_6\text{CoO}_4$  deteriorates quickly over cycles (76.4 wt%, *i.e.* 95.5 mol%, in the first cycle to 30.5 wt%, *i.e.* 38.1 mol% after 10 cycles), owing to the irreversible oxidation of  $\text{Co}^{2+}$  to  $\text{Co}^{3+}$  by the  $\text{O}_2$  present under the testing conditions.<sup>127</sup>

The cyclic stability of Li-transition metal oxides is either poor or unreported. Doping a second transition metal (*e.g.* Mn, Fe or Ni)<sup>128</sup> and alkali metal nitrates ( $\text{MNO}_3$ , M = Li, Na, K)<sup>129</sup> has been proven effective for improving the capture capacity (from 23 wt% to 35 wt%, *i.e.* 57 to 87.1 mol%) and cyclic stability of  $\text{Li}_2\text{CuO}_2$ . Again, the improvement is by virtue of improving the ionic conductivity of the product layers.

Lastly, trilithium borate ( $\text{Li}_3\text{BO}_3$ ) has been synthesised by precipitation using  $\text{LiOH}$  and  $\text{H}_3\text{BO}_3$  as the precursors.<sup>131</sup>  $\text{Li}_3\text{BO}_3$  captures  $\text{CO}_2$  with a stoichiometric uptake capacity of 41.4 wt%:



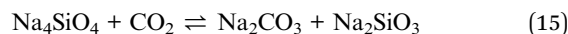
With a reported experimental  $\text{CO}_2$  uptake of 35.4 wt% (51.2 mol%), measured after 4 h in pure  $\text{CO}_2$  at 580 °C. The poor cyclic stability of  $\text{Li}_3\text{BO}_3$  could be improved by  $\text{NaNO}_2$  or  $\text{KNO}_2$  doping, which significantly accelerates product layer diffusion as the dopant salts form a molten layer. Interestingly, the 10 mol% (Na-K) $\text{NO}_2$  doped  $\text{Li}_3\text{BO}_3$  showed an experimental uptake of 47.2 wt% (68.3 mol%), exceeding the stoichiometric maximum capacity predicted by eqn (16). This was because the alkali metal nitrites promoted the deep carbonation of lithium borate:



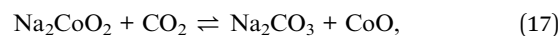
Resulting in improved stoichiometric uptake capacities of 69.1 and 55.4 wt%, respectively.

## 4.2 Na based sorbents

Na based sorbents have similar chemical formulae as the Li based ones (see Section 4.1). Because sodium is earth-abundant, Na based sorbents are potentially more economical. On the other hand, sodium is heavier and therefore, the stoichiometric  $\text{CO}_2$  uptake capacity of Na based sorbents are generally lower than that of the Li equivalents in terms of wt%. Experimentally, sodium orthosilicate, sodium zirconate and other sodium metal oxides have shown promising  $\text{CO}_2$  capture performance over a wide temperature range (from near-ambient temperatures to 850 °C):



These compounds generally exhibit good cyclic stability, with the exception of undoped  $\text{Na}_2\text{CoO}_2$ :



which shows limited experimental  $\text{CO}_2$  uptake (3.3–5.0 wt%, *i.e.* 22.0–33.3 mol%) that is substantially below the stoichiometric capacity of 15 wt%.<sup>132</sup>

Similar to Li based sorbents, Na based sorbents can be prepared by solid-state reactions between metal precursors, *e.g.*  $\text{Na}_2\text{SiO}_3 + \text{NaOH}$ ,<sup>133</sup>  $\text{Na}_2\text{CO}_3 + \text{ZrO}_2$ ,<sup>134</sup> and  $\text{Na}_2\text{CO}_3 + \text{CoCO}_3$ ,<sup>132</sup> as well as by wet-chemistry methods such as sol-gel synthesis.<sup>135,136</sup>

$\text{Na}_4\text{SiO}_4$  was found to perform well above 750 °C, showing a maximum uptake of 19.2 wt% (80.3 mol%, with a stoichiometric uptake capacity of 23.9 wt%) at 840 °C.<sup>133</sup> One approach to improve the low-temperatures performance of  $\text{Na}_4\text{SiO}_4$  is doping alkali carbonates ( $\text{M}_2\text{CO}_3$ , M = Li, Na, K), which promotes the diffusion of  $\text{O}_2^-$  through the molten carbonate layer. The promotional effects follow the order  $\text{K}_2\text{CO}_3 > \text{Na}_2\text{CO}_3 > \text{Li}_2\text{CO}_3$ , probably because of the increased basicity from Li to K.<sup>133</sup> Although the dopants decrease the mass-based  $\text{CO}_2$  uptake capacity of the  $\text{Na}_4\text{SiO}_4$  sorbent, doping significantly improved carbonation rates even below 700 °C. In particular,  $\text{K}_2\text{CO}_3$ -doped  $\text{Na}_4\text{SiO}_4$  showed 4.7 wt% (19.7 mol%)  $\text{CO}_2$  uptake at 300 °C, doubling that of undoped  $\text{Na}_4\text{SiO}_4$ .

During the carbonation of  $\text{Na}_2\text{ZrO}_3$ , the solid products could form a mesoporous layer with high gas permeability, as depicted in Fig. 13a and b. As a result, the  $\text{Na}_2\text{ZrO}_3$  sorbents do not

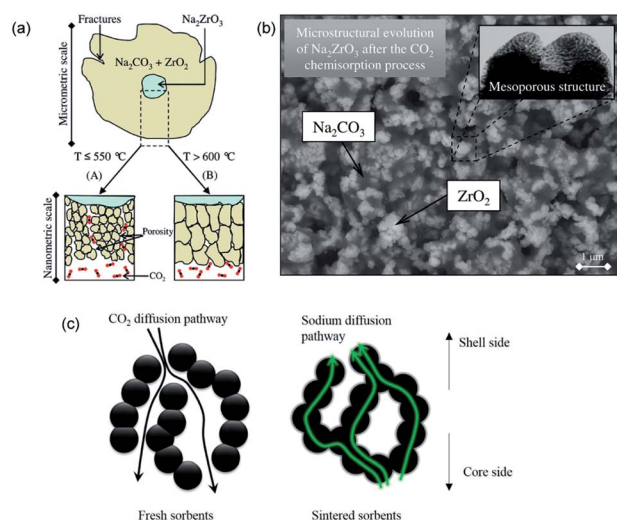


Fig. 13 (a) Scheme of the  $\text{CO}_2$  uptake on  $\text{Na}_2\text{ZrO}_3$  at different temperatures. Reprinted with permission<sup>134</sup> copyright 2021 American Chemical Society (b) SEM image of growth of  $\text{ZrO}_2$  and  $\text{Na}_2\text{CO}_3$  after the carbonation of  $\text{Na}_2\text{ZrO}_3$ . Reprinted with permission<sup>134</sup> copyright 2021 American Chemical Society (c) Scheme of the  $\text{CO}_2$  and sodium diffusion in the sorbent under fresh and sintered state. Reprinted with permission<sup>135</sup> copyright 2021 Elsevier.



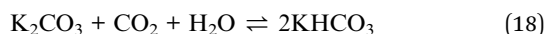


experience significant product layer diffusion resistance, as long as the product layer does not sinter.<sup>137</sup> Nevertheless, increasing the initial porosity of Na<sub>2</sub>ZrO<sub>3</sub>, *e.g.* by synthesising the sorbent using sol-gel method, could still render improvements in CO<sub>2</sub> uptake and cyclic stability during high temperature operations.<sup>135</sup> The best performance was achieved by the Na<sub>2</sub>ZrO<sub>3</sub> prepared from sodium oxalate and Zr(NO<sub>3</sub>)<sub>4</sub>, showing an uptake of 22.6 wt% (95.0 mol%, with a stoichiometric uptake of 23.8 wt%), which was largely maintained over 5 successive cycles. Ji *et al.* attributed the high performance to the partly sintered product layer, which facilitates fast sodium diffusion as a form of mass transfer enhancement, as depicted in Fig. 13c.

For NaCoO<sub>2</sub>, substitutionally doping the Co sites with Fe could substantially improve the redox activity, ionic conductivity and therefore CO<sub>2</sub> capture performance of the ternary oxide. For instance, NaCo<sub>0.7</sub>Fe<sub>0.3</sub>O<sub>2</sub> showed improved capacity of 10.6 wt% (70.7 mol%) in 20% CO<sub>2</sub> at 700 °C (*cf.* 3.3 wt%, 22.0 mol% without doping).<sup>132</sup> The CO<sub>2</sub> uptake could be further improved to 11.1 wt% (74.0 mol%) in the presence of 5% O<sub>2</sub> at 800 °C, because the presence of O<sub>2</sub> would stabilise the NaCoO<sub>2</sub> phase.

### 4.3 K based sorbents

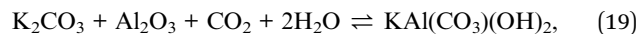
Unlike lithium and sodium based sorbents, whose functional forms are mixed oxides, potassium based sorbents primarily function in the form of K<sub>2</sub>CO<sub>3</sub> and take up CO<sub>2</sub> by forming bicarbonate in the presence of moisture with a stoichiometric CO<sub>2</sub> uptake capacity of 31.8 wt%:



Experimentally, the carbonation and regeneration of K<sub>2</sub>CO<sub>3</sub> occur at 50–60 °C and around 200 °C, respectively. This makes

K<sub>2</sub>CO<sub>3</sub> an excellent candidate for CO<sub>2</sub> capture at near-ambient temperatures. The practically achievable CO<sub>2</sub> uptake by K<sub>2</sub>CO<sub>3</sub> is as high as 28.7 wt% (90.3 mol%).<sup>138</sup> However, the cyclic stability of K<sub>2</sub>CO<sub>3</sub> is limited.

To improve the cyclic stability, researchers have impregnated K<sub>2</sub>CO<sub>3</sub> on various types of high melting point supports. The most readily available support material is alumina.<sup>139</sup> However, the interaction between Al<sub>2</sub>O<sub>3</sub> and K<sub>2</sub>CO<sub>3</sub> would form the thermally stable KAl(CO<sub>3</sub>)(OH)<sub>2</sub>:<sup>140</sup>



which results in drastic capacity loss (9.6 wt%, to 4.8 wt%, *i.e.* 30.2 mol% to 15.1 mol%) after only 3 cycles.<sup>141</sup> One way to avoid KAl(CO<sub>3</sub>)(OH)<sub>2</sub> formation is to restrict the operation to ambient temperatures and perform pressure swing cycles instead.<sup>142</sup> However, the cost-benefit of doing pressure swing CO<sub>2</sub> capture must be further justified, as pressure swing processes are often associated with high energy penalties and additional costs arising from gas compression.

Alternatively, support materials that do not react with K<sub>2</sub>CO<sub>3</sub> can be used, such as silicates (*e.g.* Al<sub>6</sub>Si<sub>2</sub>O<sub>13</sub>, CaSiO<sub>3</sub>, ZrSiO<sub>4</sub>, which inert towards K<sub>2</sub>CO<sub>3</sub>),<sup>141</sup> ZrO<sub>2</sub> (*ref.* 139) and porous carbon.<sup>143</sup> In all cases, stable performance over 10 cycles can be achieved at the expense of reduced CO<sub>2</sub> uptake (6.5–11.8 wt%, *i.e.* 20.4–37.1 mol% *cf.* the stoichiometric maximum of 31.8 wt%). Most interestingly, Yang *et al.*<sup>143</sup> impregnated K<sub>2</sub>CO<sub>3</sub> on carbon aerogels, which possess extremely specific high surface areas (350 to 450 m<sup>2</sup> g<sup>-1</sup>) and provide additional physisorption sites for CO<sub>2</sub>. As a result, they reported the highest CO<sub>2</sub> uptake of 9.2–11.8 wt% (28.9–37.1 mol%), amongst the highest of all supported K<sub>2</sub>CO<sub>3</sub> sorbents. Nevertheless, the

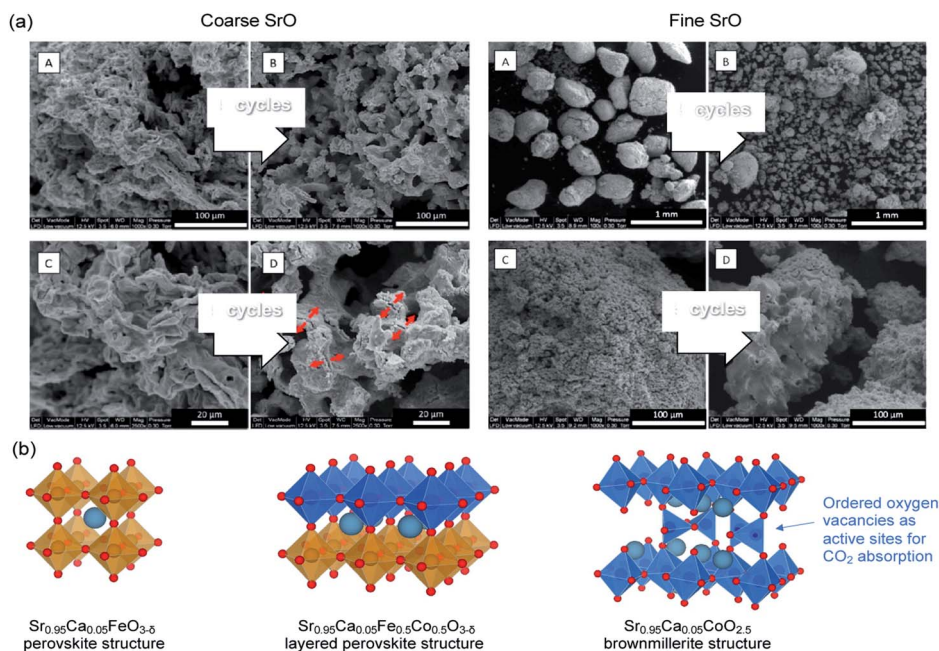


Fig. 14 (a) SEM images of coarse and fine SrO particles before (A & C) and after five cycles (B & D) of carbonation–calcination at 1100 °C (b) Sr<sub>0.95</sub>Ca<sub>0.05</sub>Fe<sub>0.5</sub>Co<sub>0.5</sub>O<sub>3-δ</sub> perovskite with a layered structure and its phase segregation to a Fe-rich and a Co-rich phase. The undercoordinated Co sites are considered to be the preferential sites for CO<sub>2</sub> absorption. Reprinted with permission<sup>144</sup> copyright 2021 American Chemical Society.

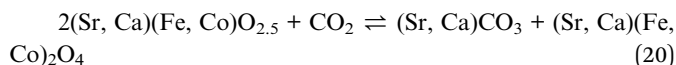


application of the carbon based supports for CO<sub>2</sub> capture must be further validated under realistic operation conditions, considering the lack of CO<sub>2</sub> selectivity by the physisorption process and the lack of stability of carbon in the presence of oxygen, a common component in combustion flue gases.

#### 4.4 Sr based sorbents

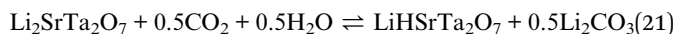
SrO can function by itself as a high temperature (>1000 °C) CO<sub>2</sub> sorbent with relatively high initial CO<sub>2</sub> uptake. Indeed, Miccio *et al.*<sup>144</sup> prepared SrO sorbents with mean particle size of 0.5 mm and 5.0 mm by calcining SrCO<sub>3</sub> and wet-granulation (Fig. 14a). The SrO sorbents with mean particle size of 0.5 mm and 5.0 mm had specific surface areas of 1.3 and 2.2 m<sup>2</sup> g<sup>-1</sup>, respectively.<sup>144</sup> Both the fine, low surface area and coarse, high surface area SrO particles showed high initial CO<sub>2</sub> uptake capacities of 37.1 and 30.5 wt% (87.3 and 48.2 mol%), respectively, when tested in 50% CO<sub>2</sub> at 1100 °C. However, the uptake capacity rapidly dropped over cycles due to sintering. The attempt to support SrO<sub>2</sub> on Al<sub>2</sub>O<sub>3</sub> by mechanical mixing resulted in the formation of Sr<sub>3</sub>Al<sub>2</sub>O<sub>6</sub> and SrAl<sub>2</sub>O<sub>4</sub>, both appeared beneficial to the sorbent's cyclic stability, at the expense of reducing the capture capacity to 8.7–9.3 wt% (20.5–21.9 mol%).

Alternatively, Sr-containing perovskites, in which Sr occupies the A sites in the ABO<sub>3</sub> lattice, can be used directly as CO<sub>2</sub> sorbents. These perovskite structured sorbents are typically prepared *via* sol-gel synthesis.<sup>145</sup> The A site and B site occupancies of the perovskites can be flexibly adjusted by varying the compositions of the metal precursors during the sol-gel synthesis. The site occupancies in turn influence the CO<sub>2</sub> capture performance. For example, La<sub>0.1</sub>Sr<sub>0.9</sub>Co<sub>0.5</sub>Fe<sub>0.5</sub>O<sub>3-δ</sub> was found to capture more CO<sub>2</sub> (17.3 wt%, *i.e.* 83.6 mol%) than Sr<sub>0.95</sub>Ca<sub>0.05</sub>Fe<sub>0.5</sub>Co<sub>0.5</sub>O<sub>3-δ</sub> (4.48 wt%, *i.e.* 18.3–33.2 mol%).<sup>146,147</sup> However, further increasing the Ca occupancy in the A site (replacing more Sr) to Sr<sub>0.5</sub>Ca<sub>0.5</sub>Fe<sub>0.5</sub>Co<sub>0.5</sub>O<sub>3-δ</sub> could improve the uptake to 17 wt% (62.3 mol%).<sup>147</sup> Such improvement was attributed to the fact that Sr<sub>0.5</sub>Ca<sub>0.5</sub>Fe<sub>0.5</sub>Co<sub>0.5</sub>O<sub>3-δ</sub> with δ ≈ 0.53 corresponds to a brownmillerite structure (see Fig. 14b) with ordered oxygen vacancies, which are regarded by many to be beneficial to CO<sub>2</sub> uptake:<sup>146,148</sup>



Adjusting the B-site occupancies could also influence the capture performance. Lu *et al.*<sup>149</sup> synthesised SrCo<sub>1-2x</sub>(Fe, Nb)<sub>x</sub>O<sub>3-δ</sub> with equimolar amount of Fe and Nb by solid-state reactions between SrCO<sub>3</sub>, Co<sub>3</sub>O<sub>4</sub> (or Co<sub>2</sub>O<sub>3</sub>), Fe<sub>2</sub>O<sub>3</sub>, and Nb<sub>2</sub>O<sub>5</sub>. For x = 0.05 and 0.10, the freshly synthesised sorbents showed CO<sub>2</sub> uptake of 13.1 wt% (55.5 mol%) and 11.1 wt% (47.0 mol%), respectively, when evaluated in 75% CO<sub>2</sub> at 925 °C. Here, the increased B site occupancy by Nb enhanced the acidity and reduced the activity of the perovskite towards carbonation.<sup>150</sup>

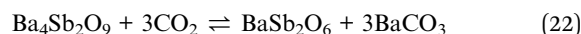
Beyond the cubic-perovskite structure, a Ruddlesden-Popper (RP) structured (A'<sub>2</sub>[A<sub>n-1</sub>B<sub>n</sub>O<sub>3n+1</sub>]) Li<sub>2</sub>SrTa<sub>2</sub>O<sub>7</sub> sorbent was prepared by Galven *et al.* by solid state synthesis.<sup>151</sup> This RP phase achieved 4.90 wt% (96.1 mol%) uptake (with a stoichiometric uptake of 5.11 wt%) after 15 h in humid CO<sub>2</sub> at 140 °C, 30 bar pressure:



In addition, the Li<sub>2</sub>SrTa<sub>2</sub>O<sub>7</sub> sorbent exhibited excellent cyclability with negligible capacity loss over 6 cycles of isothermal carbonation at 140 °C and regeneration up to 700 °C. Such performance merits further development and investigation.

#### 4.5 Ba based sorbents

Like Sr based sorbents, most studies on Ba based sorbents focus on the use of perovskite-type oxides with Ba occupying the A sites. These Ba based perovskites can be prepared by either sol-gel synthesis<sup>148</sup> or solid state reactions.<sup>152</sup> Likewise, the performance of the Ba based sorbents also depends on the site occupancies. For example, Nomura *et al.*<sup>148</sup> found that changing the Fe occupancy in (Ba<sub>0.95</sub>Ca<sub>0.05</sub>)(Co<sub>1-x</sub>Fe<sub>x</sub>)O<sub>3-δ</sub> from 0.2 to 0.9 resulted in a reduction in CO<sub>2</sub> uptake from 10.0 wt% (52.5 mol%) to 8.7 wt% (45.3 mol%). Given that BaFeO<sub>3-δ</sub> (0 < δ < 0.5) type materials are capable of reversibly changing phase between perovskite (ABO<sub>3</sub>) and brownmillerite (A<sub>2</sub>B<sub>2</sub>O<sub>5</sub>), facilitated by oxygen uptake and release, their CO<sub>2</sub> capture performance would also dependent on the oxygen partial pressure and the temperature. In general, unstable BaFeO<sub>3-δ</sub> structures correspond to improved CO<sub>2</sub> capture performance. For example, carbonating Ba<sub>0.95</sub>Ca<sub>0.05</sub>Co<sub>0.8</sub>Fe<sub>0.2</sub>O<sub>3-δ</sub> in the absence of oxygen renders an improved capture capacity of 12 wt% (62.5 mol%), owing to the thermal decomposition of perovskite to brownmillerite, which appeared as a better sorbent; this finding is in agreement with Lu *et al.*<sup>149</sup> and Fujishiro *et al.*<sup>153</sup> Yi *et al.* doped the B-sites of BaFeO<sub>3-δ</sub> with Nb,<sup>154</sup> and reported low CO<sub>2</sub> uptake (1.3 wt%, 6.9 mol%) of the doped perovskite. We suspect that the Nb dopant donates electrons to the perovskite structure, which becomes chemically stabilised and unreactive towards CO<sub>2</sub>. The most outstanding Ba based sorbents is perhaps the 6H-perovskite Ba<sub>4</sub>Sb<sub>2</sub>O<sub>9</sub> reported by Dunstan *et al.*<sup>155</sup> The authors prepared the sorbents by solid-state reaction between BaCO<sub>3</sub> and Sb<sub>2</sub>O<sub>3</sub>. Ba<sub>4</sub>Sb<sub>2</sub>O<sub>9</sub> reacts with CO<sub>2</sub> with a stoichiometric CO<sub>2</sub> uptake capacity of 14.1 wt%:



Experimentally, near-stoichiometric CO<sub>2</sub> uptake of 13.75 wt% (99.3 mol%) was observed upon carbonation at 750 °C. During long-term cyclic operation, Ba<sub>4</sub>Sb<sub>2</sub>O<sub>9</sub> showed >10 wt% (70.9 mol%) CO<sub>2</sub> uptake over 100 uptake-regeneration cycles (Fig. 15a). The excellent cyclic stability of Ba<sub>4</sub>Sb<sub>2</sub>O<sub>9</sub> originated from the sorbent's ability to fully regenerate its complete pore structure in each cycle, despite the fact that the fully carbonated sorbent showed virtually no porosity (Fig. 15b). The same authors also found Ba<sub>4</sub>Nb<sub>2-x</sub>Ta<sub>x</sub>O<sub>9</sub> materials to be poor CO<sub>2</sub> sorbents, showing uptake <0.07 wt% in 100% CO<sub>2</sub> at up to 1000 °C.<sup>156</sup>

#### 4.6 Summary and knowledge gap

Compared to the CaO and MgO based sorbents, Li, Na, K, Sr and Ba based sorbents are less commonly studied. Owing to the



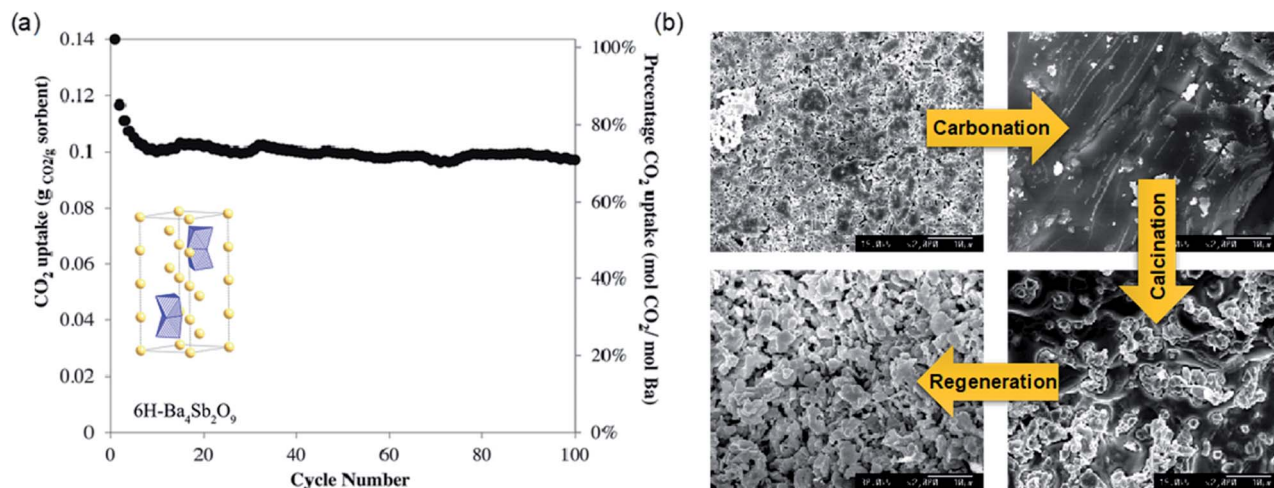


Fig. 15 (a) CO<sub>2</sub> uptake by 6H perovskite Ba<sub>4</sub>Sb<sub>2</sub>O<sub>9</sub> over 100 carbonation–calcination cycles in at TGA. (b) Surface morphology Ba<sub>4</sub>Sb<sub>2</sub>O<sub>9</sub> as it evolves over carbonation–calcination cycles. Reprinted with permission<sup>155</sup> copyright 2021 American Chemical Society.

high alkalinity of the metal sites, Li, Na, K, Sr and Ba based oxides require chemical modifications to function as reversible CO<sub>2</sub> sorbents at reasonable temperatures. These chemical modifications refer to a large pool of candidate sorbent compositions. Whilst many of these sorbents behave similarly during CO<sub>2</sub> uptake (*e.g.*, the double shell model for lithium silicates, lithium zirconates, sodium silicates and sodium zirconates), significantly more research is needed to fully understand and rationalise the behaviour of these mixed oxide sorbents in relation to their chemical composition, structure and synthesis methods. Following the discussion above, we summarise the following knowledge gaps for Li, Na, K, Sr and Ba based sorbents:

- The effect of strain development on the product layers during carbonation (*e.g.* following the double shell model depicted in Fig. 12a) is not well understood.
- Most of the sorbents discussed in this section have not been tested under practical CO<sub>2</sub> capture conditions, *i.e.* carbonation in 5–15% CO<sub>2</sub> (in the presence of moisture) and calcination in pure CO<sub>2</sub>.
- The test conditions employed by different studies are inconsistent, making it difficult to make fair comparisons.
- Most CO<sub>2</sub> uptake tests were done in TGA, whilst some sorbents have only been studied for 1 carbonation cycle or by temperature programme carbonation.
- The synthesis parameters have not been sufficiently explored to identify optimal synthesis procedures.
- The cost-benefit of synthesising sorbents with complex structures and compositions must be justified.

## 5 Challenges and opportunities

This review discusses the recent advances in developing synthetic oxide sorbents for CO<sub>2</sub> capture. The CO<sub>2</sub> uptake ability of these sorbents originates from the alkalinity of the group 1 and group 2 metals. Because of reasons associated with cost, natural abundance and the performance of the natural mineral-

derived sorbents, different classes of solid oxide sorbents have received varying extents of research attention and have reached different levels of technological maturity. Specifically, CaO based sorbents can be produced at large quantities from low-cost Ca sources (*e.g.* limestone), and have been extensively tested over a wide range of scales (from TGA to pilot plants) in realistic flue gas compositions. In contrast, all non-CaO based sorbents require specific chemical modifications to achieve improved CO<sub>2</sub> capture kinetics and capacity. Furthermore, the lack of testing standards for the non-CaO sorbents makes it difficult to have meaningful comparisons between different studies, even if they report similar chemical formulations. Addressing the lack of testing standards with priority will allow the field to develop faster and more efficiently.

There is also much commonality between different classes of sorbents. For instance, the carbonation of almost all solid oxide sorbents depends on the porosity and the mass transfer through the carbonated product layer. However, maintaining the porous structure of a solid material while it undergoes many cycles of phase changes (*i.e.* between oxides and carbonates) is technically challenging. Indeed, much research has been devoted to improving the cyclic stability of the solid oxide sorbents through synthetic approaches. One of the key methods involves mixing the active sorbent phases with thermal stabilisers such as Al<sub>2</sub>O<sub>3</sub> and ZrO<sub>2</sub>. Here, the chemical interaction between the active component (solid bases) and the thermal stabilizer phases (typically acidic oxides) must be understood and taken into consideration, as these interactions could potentially form inert phases (*e.g.* Ca<sub>12</sub>Al<sub>14</sub>O<sub>33</sub> and KAl(CO<sub>3</sub>)(OH)<sub>2</sub>) to dilute the CO<sub>2</sub> uptake capacity of the composite sorbents.

The synthetic approaches to improve the CO<sub>2</sub> uptake kinetics are also equally applicable across different classes of sorbents. For example, doping the sorbent surface with low-melting point salts could result in the formation of a molten salt layer during high temperature operation. Consequently, the mass transfer of CO<sub>2</sub> through the carbonate product layer can be drastically improved. Doping redox active metals such as Fe<sup>3+</sup> could further





enhance the mass transfer, which is governed by ionic diffusion through the molten layer, thereby achieving fast CO<sub>2</sub> capture and high CO<sub>2</sub> uptake capacity. For sorbents that do not rely on the functioning of the molten salt layer, it is generally beneficial to prepare sorbents with high specific surface area and high porosity. To this end, the knowledge in preparing CaO based sorbents, e.g. the effect of synthesis parameters on the morphological properties of the final products, can be adapted for improving the performance of other types of oxide sorbents for a wide range of process applications.

For applications where the capturing and regeneration should take place at moderate to low temperatures, there is also an opportunity to hybridise metal oxides with membranes, polymers, and carbon-based materials to yield synergistic effects and enhanced sorbent performance.<sup>157–159</sup> For instance, it has been reported that doping membranes with metal oxides resulted in improved CO<sub>2</sub> uptake. Doped membranes with polar –OH group on the surfaces can increase the membrane sorbent's reactivity with CO<sub>2</sub> molecules – as CO<sub>2</sub> molecules and metal oxide act as electron acceptors and donors, respectively, the selectivity and permeability of the oxide-doped membrane towards CO<sub>2</sub> molecules can be effectively increased.<sup>160–162</sup> On the other hand, more research effort is required to improve the cyclic regenerability and durability of these composite sorbent materials.

Beyond experimental approaches, the emerging of computational chemistry has offered opportunity to accelerate sorbent formulation with unprecedented efficiencies. In fact, computational approaches have been widely adopted by chemists developing solid sorbents based on MOFs, zeolites and carbon materials,<sup>163–166</sup> including high-throughput screening studies that explored candidate sorbent materials in computational databases.<sup>167–170</sup> For solid oxide sorbents, *ab initio* computational studies would in the first instance rely on density functional theory (DFT) calculations to predict the properties of the oxides and the active sites for CO<sub>2</sub> uptake. Dunstan *et al.* has conducted a pioneering high throughput screening of oxidic CO<sub>2</sub> sorbent materials using the Materials Project database and identified Na<sub>3</sub>SbO<sub>4</sub> and Li<sub>5</sub>FeO<sub>4</sub> to be promising CO<sub>2</sub> sorbents.<sup>19</sup> Similarly, the computational screening by Gaultois *et al.* found Li<sub>5</sub>SbO<sub>5</sub> as a potential sorbent, which showed satisfactory CO<sub>2</sub> uptake performance (~72% of its stoichiometric uptake capacity) over 25 cycles.<sup>130</sup> At present, there remains a gap between the thermochemical material properties that are computationally predicted and those experimentally measured. Such gap could potentially hinder the effective of the computational approaches to discover and develop new sorbents. However, with the rapid advancement in computational methods to simulate detailed chemical and physical phenomena, we anticipate computer-aided materials design methods to play major roles in the future development of solid oxide CO<sub>2</sub> sorbents.

## Author contributions

Ribooga Chang: data curation, formal analysis, writing – original draft, writing – review & editing; Xianyue Wu: data curation,

formal analysis, writing – original draft, writing – review & editing; Ocean Cheung: conceptualization, funding acquisition, supervision, writing – review & editing; Wen Liu: conceptualization, funding acquisition, supervision, writing – review & editing.

## Conflicts of interest

There are no conflicts to declare.

## Acknowledgements

R. C. and O. C. thank the Swedish Foundation for International Cooperation in Research and Higher Education (STINT) (Grant no. IB2019-8184), the Swedish Research Council (Grant no. 2020-04029) and Swedish Research Council for Sustainable Development (FORMAS, Grant no. 2018-00651) for their financial support. W. L. acknowledges the financial support by National Research Foundation of Singapore under its Campus of Research Excellence and Technological Enterprise (CRETE) programme.

## References

- 1 M. Z. Akram, V. Atla, A. Nambo, B. P. Ajayi, J. B. Jasinski, J. He, J. R. Gong and M. Sunkara, *Nano Lett.*, 2018, **18**, 4891–4899.
- 2 G. D. Farquhar, M. L. Goulden, M. J. R. Fasham, M. Heimann, V. J. Jaramillo, H. S. Khesghi, C. Le Quéré, R. J. Scholes and D. W. R. Wallace, *IPCC*, 2001.
- 3 M. Bui, C. S. Adjiman, A. Bardow, E. J. Anthony, A. Boston, S. Brown, P. S. Fennell, S. Fuss, A. Galindo, L. A. Hackett, J. P. Hallett, H. J. Herzog, G. Jackson, J. Kemper, S. Krevor, G. C. Maitland, M. Matuszewski, I. S. Metcalfe, C. Petit, G. Puxty, J. Reimer, D. M. Reiner, E. S. Rubin, S. A. Scott, N. Shah, B. Smit, J. P. M. Trusler, P. Webley, J. Wilcox and N. Mac Dowell, *Energy Environ. Sci.*, 2018, **11**, 1062–1176.
- 4 R. Stanger, T. Wall, R. Spörl, M. Paneru, S. Grathwohl, M. Weidmann, G. Scheffknecht, D. McDonald, K. Myöhänen, J. Ritvanen, S. Rahiala, T. Hyppänen, J. Mletzko, A. Kather and S. Santos, *Int. J. Greenhouse Gas Control*, 2015, **40**, 55–125.
- 5 M. Finkenrath, *Chem. Eng. Technol.*, 2012, **35**, 482–488.
- 6 A. Brunetti, F. Scura, G. Barbieri and E. Drioli, *J. Membr. Sci.*, 2010, **359**, 115–125.
- 7 F. Vega, A. Sanna, B. Navarrete, M. M. Maroto-Valer and V. J. Cortés, *Greenhouse Gases: Sci. Technol.*, 2014, **4**, 707–733.
- 8 S. Kumar, R. Srivastava and J. Koh, *J. CO<sub>2</sub> Util.*, 2020, **41**, 101251.
- 9 Z. Hu, Y. Wang, B. B. Shah and D. Zhao, *Adv. Sustainable Syst.*, 2019, **3**, 1800080.
- 10 O. Cheung and N. Hedin, *RSC Adv.*, 2014, **4**, 14480–14494.
- 11 M. Ding, R. W. Flaig, H.-L. Jiang and O. M. Yaghi, *Chem. Soc. Rev.*, 2019, **48**, 2783–2828.





- 12 O. K. Farha, A. Özgür Yazaydın, I. Eryazici, C. D. Malliakas, B. G. Hauser, M. G. Kanatzidis, S. T. Nguyen, R. Q. Snurr and J. T. Hupp, *Nat. Chem.*, 2010, **2**, 944–948.
- 13 L. H. Xie, M. M. Xu, X. M. Liu, M. J. Zhao and J. R. Li, *Adv. Sci.*, 2020, **7**, 1901758.
- 14 S. Mukherjee, S. Sharma and S. K. Ghosh, *APL Mater.*, 2019, **7**, 050701.
- 15 N. Ghasem, in *Advances in Carbon Capture*, 2020, pp. 479–501.
- 16 C. Song, Q. Liu, S. Deng, H. Li and Y. Kitamura, *Renewable Sustainable Energy Rev.*, 2019, **101**, 265–278.
- 17 G. Ji and M. Zhao, *Recent Advances in Carbon Capture and Storage*, 2017, ch. 3, DOI: DOI: 10.5772/65723.
- 18 U. W. R. Siagian, A. Raksajati, N. F. Himma, K. Khoiruddin and I. G. Wenten, *J. Nat. Gas Sci. Eng.*, 2019, **67**, 172–195.
- 19 M. T. Dunstan, A. Jain, W. Liu, S. P. Ong, T. Liu, J. Lee, K. A. Persson, S. A. Scott, J. S. Dennis and C. P. Grey, *Energy Environ. Sci.*, 2016, **9**, 1346–1360.
- 20 J. Blamey, E. J. Anthony, J. Wang and P. S. Fennell, *Prog. Energy Combust. Sci.*, 2010, **36**, 260–279.
- 21 C. C. Dean, J. Blamey, N. H. Florin, M. J. Al-Jeboori and P. S. Fennell, *Chem. Eng. Res. Des.*, 2011, **89**, 836–855.
- 22 M. Reitz, M. Junk, J. Ströhle and B. Eppele, *Int. J. Greenhouse Gas Control*, 2016, **54**, 272–281.
- 23 J. A. Duffy, *J. Am. Ceram. Soc.*, 1997, **80**, 1416–1420.
- 24 J. A. Duffy, *Geochim. Cosmochim. Acta*, 1993, **57**, 3961–3970.
- 25 J. Wang, L. Huang, R. Yang, Z. Zhang, J. Wu, Y. Gao, Q. Wang, D. O'Hare and Z. Zhong, *Energy Environ. Sci.*, 2014, **7**, 3478–3518.
- 26 M. T. Dunstan, F. Donat, A. H. Bork, C. P. Grey and C. R. Müller, *Chem. Rev.*, 2021, **121**, 12681–12745.
- 27 A. Perejón, L. M. Romeo, Y. Lara, P. Lisbona, A. Martínez and J. M. Valverde, *Appl. Energy*, 2016, **162**, 787–807.
- 28 M. C. Romano, I. Martínez, R. Murillo, B. Arstad, R. Blom, D. C. Ozcan, H. Ahn and S. Brandani, *Energy Procedia*, 2013, **37**, 142–150.
- 29 A. M. Kierzkowska, R. Pacciani and C. R. Müller, *J. Mater. Chem. A*, 2013, **6**, 1130–1148.
- 30 T. Xu, X. Wang, B. Xiao and W. Liu, *Chem. Eng. J.*, 2021, **425**, 131522.
- 31 IEA, *The challenge of reaching zero emissions in heavy industry*, IEA, Paris, 2020, <https://www.iea.org/articles/the-challenge-of-reaching-zero-emissions-in-heavy-industry>.
- 32 S. Gardarsdottir, E. De Lena, M. Romano, S. Roussanaly, M. Voldsund, J.-F. Pérez-Calvo, D. Berstad, C. Fu, R. Anantharaman, D. Sutter, M. Gazzani, M. Mazzotti and G. Cinti, *Energies*, 2019, **12**, 542.
- 33 M. C. Romano, M. Spinelli, S. Campanari, S. Consonni, G. Cinti, M. Marchi and E. Borgarello, *Energy Procedia*, 2013, **37**, 7091–7099.
- 34 B. Arias, M. E. Diego, J. C. Abanades, M. Lorenzo, L. Diaz, D. Martínez, J. Alvarez and A. Sánchez-Biezma, *Int. J. Greenhouse Gas Control*, 2013, **18**, 237–245.
- 35 M.-H. Chang, W.-C. Chen, C.-M. Huang, W.-H. Liu, Y.-C. Chou, W.-C. Chang, W. Chen, J.-Y. Cheng, K.-E. Huang and H.-W. Hsu, *Energy Procedia*, 2014, **63**, 2100–2108.
- 36 B. Arias, M. Alonso and C. Abanades, *Ind. Eng. Chem. Res.*, 2017, **56**, 2634–2640.
- 37 M. Erans, M. Jeremias, V. Manovic and E. J. Anthony, *J. Visualized Exp.*, 2017, **128**, e56122.
- 38 A. de la Calle Martos, J. M. Valverde, P. E. Sanchez-Jimenez, A. Perejon, C. Garcia-Garrido and L. A. Perez-Maqueda, *Phys. Chem. Chem. Phys.*, 2016, **18**, 16325–16336.
- 39 C. Zhongxiang, H. S. Song, M. Portillo, C. J. Lim, J. R. Grace and E. J. Anthony, *Energy Fuels*, 2009, **23**, 1437–1444.
- 40 H. Sun, C. Wu, B. Shen, X. Zhang, Y. Zhang and J. Huang, *Mater. Today Sustain.*, 2018, **1–2**, 1–27.
- 41 Y. Hu, H. Lu, W. Liu, Y. Yang and H. Li, *Chem. Eng. J.*, 2020, **396**, 125253.
- 42 J. M. Valverde, *J. Nanopart. Res.*, 2018, **20**, 39.
- 43 V. Manovic and E. J. Anthony, *Ind. Eng. Chem. Res.*, 2010, **49**, 9105–9110.
- 44 S. Yang and Y. Xiao, *Ind. Eng. Chem. Res.*, 2008, **47**, 4043–4048.
- 45 J. Yin, C. Zhang, C. Qin, W. Liu, H. An, G. Chen and B. Feng, *Chem. Eng. J.*, 2012, **198–199**, 38–44.
- 46 B. Arias, G. S. Grasa and J. C. Abanades, *Chem. Eng. J.*, 2010, **163**, 324–330.
- 47 A. N. Antzara, A. Arregi, E. Heracleous and A. A. Lemonidou, *Chem. Eng. J.*, 2018, **333**, 697.
- 48 H. Guo, S. Yan, Y. Zhao, X. Ma and S. Wang, *Chem. Eng. J.*, 2019, **359**, 542–551.
- 49 J. Sun, W. Wang, Y. Yang, S. Cheng, Y. Guo, C. Zhao, W. Liu and P. Lu, *Fuel*, 2020, **266**, 117056.
- 50 V. Manovic and E. J. Anthony, *Environ. Sci. Technol.*, 2008, **42**, 4170–4174.
- 51 K. Labus, *Materials*, 2021, **14**, 548.
- 52 A. H. Soleimanisalim, M. H. Sedghkerdar, D. Karami and N. Mahinpey, *J. Nat. Gas Sci. Eng.*, 2016, **36**, 1056–1061.
- 53 S. M. Hashemi, D. Karami and N. Mahinpey, *Fuel*, 2020, **269**, 117432.
- 54 A. Kurlov, A. Armutlulu, F. Donat, A. R. Studart and C. R. Müller, *Ind. Eng. Chem. Res.*, 2019, **59**, 7182–7188.
- 55 H. Sun, J. Wang, J. Zhao, B. Shen, J. Shi, J. Huang and C. Wu, *Appl. Catal., B*, 2019, **244**, 63–75.
- 56 M. Vall, J. Hultberg, M. Strømme and O. Cheung, *RSC Adv.*, 2019, **9**, 20273–20280.
- 57 C. Luo, Y. Zheng, N. Ding, Q. L. Wu and C. G. Zheng, *Chin. Chem. Lett.*, 2011, **22**, 615–618.
- 58 H. J. Yoon and K. B. Lee, *Chem. Eng. J.*, 2019, **355**, 850–857.
- 59 K. S. Sultana, D. T. Tran, J. C. Walmsley, M. Rønning and D. Chen, *Ind. Eng. Chem. Res.*, 2015, **54**, 8929–8939.
- 60 N. Gao, K. Chen and C. Quan, *Fuel*, 2020, **260**, 116411.
- 61 R. Han, J. Gao, S. Wei, Y. Su and Y. Qin, *J. Mater. Chem. A*, 2018, **6**, 3462–3470.
- 62 A. Armutlulu, M. A. Naeem, H. J. Liu, S. M. Kim, A. Kierzkowska, A. Fedorov and C. R. Müller, *Adv. Mater.*, 2017, **29**, 1702896.
- 63 W. Peng, Z. Xu, C. Luo and H. Zhao, *Environ. Sci. Technol.*, 2015, **49**, 8237–8245.
- 64 W. Liu, H. An, C. Qin, J. Yin, G. Wang, B. Feng and M. Xu, *Energy Fuels*, 2012, **26**, 2751–2767.



- 65 B. Azimi, M. Tahmasebpour, P. E. Sanchez-Jimenez, A. Perejon and J. M. Valverde, *Chem. Eng. J.*, 2019, **358**, 679–690.
- 66 X. Kou, C. Li, Y. Zhao, S. Wang and X. Ma, *Fuel Process. Technol.*, 2018, **177**, 210–218.
- 67 Y. Wang, W. Zhang, R. Li, W. Duan and B. Liu, *Energy Fuels*, 2016, 1248–1255.
- 68 A. N. Antzara, A. Arregi, E. Heracleous and A. A. Lemonidou, *Chem. Eng. J.*, 2018, **333**, 697–711.
- 69 H. Ping and S. Wu, *RSC Adv.*, 2015, **5**, 65052–65057.
- 70 S. Wang, H. Shen, S. Fan, Y. Zhao, X. Ma and J. Gong, *Chem. Eng. Sci.*, 2015, **135**, 532–539.
- 71 M. A. Naeem, A. Armutlulu, Q. Imtiaz and C. R. Müller, *ChemPhysChem*, 2017, **18**, 3280.
- 72 P. Jamrunroj, S. Wongsakulphasatch, A. Maneedaeng, C. K. Cheng and S. Assabumrungrat, *Powder Technol.*, 2019, **344**, 208–221.
- 73 J. Chen, T. Shi, L. Duan, Z. Sun and E. J. Anthony, *Chem. Eng. J.*, 2020, **393**, 124716.
- 74 C. Qin, W. Liu, H. An, J. Yin and B. Feng, *Environ. Sci. Technol.*, 2012, **46**, 1932–1939.
- 75 Z. Zhou, Y. Qi, M. Xie, Z. Cheng and W. Yuan, *Chem. Eng. Sci.*, 2012, **74**, 172–180.
- 76 C.-H. Huang, K.-P. Chang, C.-T. Yu, P.-C. Chiang and C.-F. Wang, *Chem. Eng. J.*, 2010, **161**, 129–135.
- 77 M. Olivares-Marín, E. M. Cuerda-Correa, A. Nieto-Sánchez, S. García, C. Pevida and S. Román, *Chem. Eng. J.*, 2013, **217**, 71–81.
- 78 M. Broda and C. R. Müller, *Fuel*, 2014, **127**, 94–100.
- 79 X. Yan, Y. Li, X. Ma, J. Zhao, Z. Wang and H. Liu, *New J. Chem.*, 2019, **43**, 5116–5125.
- 80 L. Huang, Q. Zheng, B. Louis and Q. Wang, *Energy Technol.*, 2018, **6**, 2469–2478.
- 81 S. Wei, R. Han, Y. Su, J. Gao, G. Zhao and Y. Qin, *Energy Fuels*, 2019, **33**, 5398–5407.
- 82 Y. Hu, Y. Guo, J. Sun, H. Li and W. Liu, *J. Mater. Chem. A*, 2019, **7**, 20103–20120.
- 83 B. W. Hwang, J. H. Lim, H. J. Chae, H.-J. Ryu, D. Lee, J. B. Lee, H. Kim, S. C. Lee and J. C. Kim, *Process Saf. Environ. Prot.*, 2018, **116**, 219–227.
- 84 X. Zhao, G. Ji, W. Liu, X. He, E. J. Anthony and M. Zhao, *Chem. Eng. J.*, 2018, **332**, 216–226.
- 85 A. Dal Pozzo, A. Armutlulu, M. Rekhina, P. M. Abdala and C. R. Müller, *ACS Appl. Energy Mater.*, 2019, **2**, 1295–1307.
- 86 T. Harada and T. A. Hatton, *Chem. Mater.*, 2015, **27**, 8153–8161.
- 87 J. S. Kwak, K. R. Oh, K. Y. Kim, J. M. Lee and Y. U. Kwon, *Phys. Chem. Chem. Phys.*, 2019, **21**, 20805–20813.
- 88 J. Ding, C. Yu, J. Lu, X. Wei, W. Wang and G. Pan, *Appl. Energy*, 2020, **263**, 114681.
- 89 S. Jin, K. Ho and C.-H. Lee, *Chem. Eng. J.*, 2018, **334**, 1605–1613.
- 90 H. Joo, S. J. Cho and K. Na, *J. CO<sub>2</sub> Util.*, 2017, **19**, 194–201.
- 91 A.-T. Vu, K. Ho, S. Jin and C.-H. Lee, *Chem. Eng. J.*, 2016, **291**, 161–173.
- 92 L. Wang, Z. Zhou, Y. Hu, Z. Cheng and X. Fang, *Ind. Eng. Chem. Res.*, 2017, **56**, 5802–5812.
- 93 Y. Yoo, D. Kang, E. Choi, J. Park and I.-S. Huh, *Chem. Eng. J.*, 2019, **370**, 237–250.
- 94 Y. Guo, C. Tan, P. Wang, J. Sun, W. Li, C. Zhao and P. Lu, *Chem. Eng. J.*, 2020, **379**, 122277.
- 95 Y.-D. Ding, G. Song, X. Zhu, R. Chen and Q. Liao, *RSC Adv.*, 2015, **5**, 30929–30935.
- 96 A. Hanif, S. Dasgupta and A. Nanoti, *Ind. Eng. Chem. Res.*, 2016, **55**, 8070–8078.
- 97 V. A. Tuan and C. H. Lee, *Vietnam J. Chem.*, 2018, **56**, 197–202.
- 98 P. Li, W. Liu, J. S. Dennis and H. C. Zeng, *ACS Appl. Mater. Interfaces*, 2017, **9**, 9592–9602.
- 99 P. Li, Y. Lin, R. Chen and W. Li, *Dalton Trans.*, 2020, **49**, 5183–5191.
- 100 P. Li and H. C. Zeng, *Environ. Sci. Technol.*, 2017, **51**, 12998–13007.
- 101 H.-H. Lee, J.-C. Lee, Y.-J. Joo, M. Oh and C.-H. Lee, *Appl. Energy*, 2014, **131**, 425–440.
- 102 H. Cui, Q. Zhang, Y. Hu, C. Peng, X. Fang, Z. Cheng, V. V. Galvita and Z. Zhou, *ACS Appl. Mater. Interfaces*, 2018, **10**, 20611–20620.
- 103 A. H. Bork, M. Rekhina, E. Willinger, P. Castro-Fernández, J. Drnec, P. M. Abdala and C. R. Müller, *Proc. Natl. Acad. Sci.*, 2021, **118**, e2103971118.
- 104 G. Xiao, R. Singh, A. Chaffee and P. Webley, *Int. J. Greenhouse Gas Control*, 2011, **5**, 634–639.
- 105 A.-T. Vu, Y. Park, P. R. Jeon and C.-H. Lee, *Chem. Eng. J.*, 2014, **258**, 254–264.
- 106 C. H. Lee, S. Mun and K. B. Lee, *Chem. Eng. J.*, 2014, **258**, 367–373.
- 107 K. Zhang, X. S. Li, Y. Duan, D. L. King, P. Singh and L. Li, *Int. J. Greenhouse Gas Control*, 2013, **12**, 351–358.
- 108 S. I. Jo, Y. I. An, K. Y. Kim, S. Y. Choi, J. S. Kwak, K. R. Oh and Y. U. Kwon, *Phys. Chem. Chem. Phys.*, 2017, **19**, 6224–6232.
- 109 Y. Qiao, J. Wang, Y. Zhang, W. Gao, T. Harada, L. Huang, T. A. Hatton and Q. Wang, *Ind. Eng. Chem. Res.*, 2017, **56**, 1509–1517.
- 110 Q. Wang, H. H. Tay, Z. Guo, L. Chen, Y. Liu, J. Chang, Z. Zhong, J. Luo and A. Borgna, *Appl. Clay Sci.*, 2012, **55**, 18–26.
- 111 M. L. T. Trivino, V. Hiremath and J. G. Seo, *Environ. Sci. Technol.*, 2018, **52**, 11952–11959.
- 112 S. Jin, K.-J. Ko and C.-H. Lee, *Chem. Eng. J.*, 2019, **371**, 64–77.
- 113 K. K. Han, Y. Zhou, Y. Chun and J. H. Zhu, *J. Hazard. Mater.*, 2012, **203–204**, 341–347.
- 114 X. Yang, W. Liu, J. Sun, Y. Hu, W. Wang, H. Chen, Y. Zhang, X. Li and M. Xu, *ChemSusChem*, 2016, **9**, 1607–1613.
- 115 F. Cova, G. Amica, K. Kohopää and M. V. Blanco, *Inorg. Chem.*, 2019, **58**, 1040–1047.
- 116 H. Wang, J. Zhang, G. Wang, Q. Wang and T. Song, *J. Therm. Anal. Calorim.*, 2018, **133**, 981–989.
- 117 X. Chen, Z. Xiong, Y. Qin, B. Gong, C. Tian, Y. Zhao, J. Zhang and C. Zheng, *Int. J. Hydrogen Energy*, 2016, **41**, 13077–13085.



- 118 H. A. Lara-García, O. Ovalle-Encinia, J. Ortiz-Landeros, E. Lima and H. Pfeiffer, *J. Mater. Chem. A*, 2019, **7**, 4153–4164.
- 119 K. Wang, J. Hong, Z. Zhou, Z. Lin and P. Zhao, *Energy Technol.*, 2019, **7**, 325–332.
- 120 X. Yang, W. Liu, J. Sun, Y. Hu, W. Wang, H. Chen, Y. Zhang, X. Li and M. Xu, *ChemSusChem*, 2016, **9**, 2480–2487.
- 121 M. Seggiani, E. Stefanelli, M. Puccini and S. Vitolo, *Chem. Eng. J.*, 2018, **339**, 51–60.
- 122 N. Gómez-Garduño and H. Pfeiffer, *Thermochim. Acta*, 2019, **673**, 129–137.
- 123 D. Peltzer, J. Múnera, L. Cornaglia and M. Strumendo, *Chem. Eng. J.*, 2018, **336**, 1–11.
- 124 D. Peltzer, J. Múnera and L. Cornaglia, *J. Environ. Chem. Eng.*, 2019, **7**, 102927.
- 125 N. Togashi, T. Okumura and K. Oh-Ishi, *J. Ceram. Soc. Jpn.*, 2007, **115**, 324–328.
- 126 M. V. Blanco, K. Kohopää, I. Snigireva and F. Cova, *Chem. Eng. J.*, 2018, **354**, 370–377.
- 127 E. Bernabé-Pablo, F. Plascencia-Hernández, A. Yañez-Aulestia and H. Pfeiffer, *Chem. Eng. J.*, 2020, **384**, 123291.
- 128 M. A. Martínez-Cruz, A. Yañez-Aulestia, G. Ramos-Sánchez, M. Oliver-Tolentino, M. Vera, H. Pfeiffer, D. Ramírez-Rosales and I. González, *Dalton Trans.*, 2020, **49**, 4549–4558.
- 129 A. Yañez-Aulestia, Q. Wang and H. Pfeiffer, *Phys. Chem. Chem. Phys.*, 2020, **22**, 2803–2813.
- 130 M. W. Gaultois, M. T. Dunstan, A. W. Bateson, M. S. C. Chan and C. P. Grey, *Chem. Mater.*, 2018, **30**, 2535–2543.
- 131 T. Harada and T. A. Hatton, *J. Mater. Chem. A*, 2017, **5**, 22224–22233.
- 132 E. Vera, S. García, M. M. Maroto-Valer and H. Pfeiffer, *Adsorption*, 2020, **26**, 781–792.
- 133 J. Liu, Z. Wang, Z. Wang, J. Song, G. Li, Q. Xu, J. You, H. Cheng and X. Lu, *Phys. Chem. Chem. Phys.*, 2019, **21**, 13135–13143.
- 134 L. Martínez-dlCruz and H. Pfeiffer, *J. Phys. Chem. C*, 2012, **116**, 9675–9680.
- 135 G. Ji, M. Z. Memon, H. Zhuo and M. Zhao, *Chem. Eng. J.*, 2017, **313**, 646–654.
- 136 T. Zhao, E. Ochoa-Fernández, M. Rønning and D. Chen, *Chem. Mater.*, 2007, **19**, 3294–3301.
- 137 S. Munro, M. Åhlén, O. Cheung and A. Sanna, *Chem. Eng. J.*, 2020, **388**, 124284.
- 138 C. Zhao, X. Chen and C. Zhao, *Int. J. Greenhouse Gas Control*, 2010, **4**, 655–658.
- 139 S. C. Lee, H. J. Chae, S. J. Lee, Y. H. Park, C. K. Ryu, C. K. Yi and J. C. Kim, *J. Mol. Catal. B: Enzym.*, 2009, **56**, 179–184.
- 140 S. C. Lee and J. C. Kim, *Catal. Surv. Asia*, 2007, **11**, 171–185.
- 141 M. S. Cho, S. C. Lee, H. J. Chae, Y. M. Kwon, J. B. Lee and J. C. Kim, *Process Saf. Environ. Prot.*, 2018, **117**, 296–306.
- 142 S. Boonprasop, B. Chalermisinsuwan and P. Piumsomboon, *J. Taiwan Inst. Chem. Eng.*, 2018, **88**, 215–225.
- 143 G. Yang, H. Luo, T. Ohba and H. Kanoh, *Int. J. Chem. Eng.*, 2016, **2016**, 4012967.
- 144 F. Miccio, A. N. Murri and E. Landi, *Ind. Eng. Chem. Res.*, 2016, **55**, 6696–6707.
- 145 Q. Yang and Y. S. Lin, *Ind. Eng. Chem. Res.*, 2006, **45**, 6302–6310.
- 146 Z. Homonnay, K. Nomura, G. Juhász, M. Gál, K. Sólmos, S. Hamakawa, T. Hayakawa and A. Vértés, *Chem. Mater.*, 2002, **14**, 1127–1135.
- 147 G. Juhász, Z. o. Homonnay, K. Nomura, T. Hayakawa, S. Hamakawa and A. Vértés, *Solid State Ionics*, 2001, **139**, 219–231.
- 148 K. Nomura, Y. Ujihira, T. Hayakawa and K. Takehira, *Appl. Catal., A*, 1996, **137**, 25–36.
- 149 H. Lu, J. P. Kim, S. H. Son and J. H. Park, *Mater. Lett.*, 2011, **65**, 2858–2860.
- 150 J. Yi, M. Schroeder, T. Weirich and J. Mayer, *Chem. Mater.*, 2010, **22**, 6246–6253.
- 151 C. Galven, J.-L. Fourquet, E. Suard, M.-P. Crosnier-Lopez and F. Le Berre, *Dalton Trans.*, 2010, **39**, 4191–4197.
- 152 B. R. Sneha and V. Thangadurai, *J. Solid State Chem.*, 2007, **180**, 2661–2669.
- 153 F. Fujishiro, K. Fukasawa and T. Hashimoto, *J. Am. Ceram. Soc.*, 2011, **94**, 3675–3678.
- 154 J. Yi, T. E. Weirich and M. Schroeder, *J. Membr. Sci.*, 2013, **437**, 49–56.
- 155 M. T. Dunstan, W. Liu, A. F. Pavan, J. A. Kimpton, C. D. Ling, S. A. Scott, J. S. Dennis and C. P. Grey, *Chem. Mater.*, 2013, **25**, 4881–4891.
- 156 M. T. Dunstan, P. D. Southon, C. J. Kepert, J. Hester, J. A. Kimpton and C. D. Ling, *J. Solid State Chem.*, 2011, **184**, 2648–2654.
- 157 M. Li, K. Huang, J. A. Schott, Z. Wu and S. Dai, *Microporous Mesoporous Mater.*, 2017, **249**, 34–41.
- 158 Y. Zhou, K. Yan, Z. Yang, R. A. Bauer, N. Hong and H. Verweij, *ACS Appl. Nano. Mater.*, 2020, **3**, 6654–6663.
- 159 H. R. Amedi and M. Aghajani, *J. Nat. Gas Sci. Eng.*, 2016, **35**, 695–702.
- 160 N. Azizi, T. Mohammadi and R. M. Behbahani, *J. Energy Chem.*, 2017, **26**, 454–465.
- 161 W. Zhu, F. Liu, M. Gou, R. Guo and X. Li, *Green Chem. Eng.*, 2021, **2**, 132–143.
- 162 W. M. Aframehr, B. Molki, R. Bagheri, P. Heidarian and S. M. Davodi, *Chem. Eng. Res. Des.*, 2020, **153**, 789–805.
- 163 C. Cazorla, S. A. Shevlin and Z. X. Guo, *J. Phys. Chem. C*, 2011, **115**, 10990–10995.
- 164 J. Yu, L.-H. Xie, J.-R. Li, Y. Ma, J. M. Seminario and P. B. Balbuena, *Chem. Rev.*, 2017, **117**, 9674–9754.
- 165 B. Vujic and A. P. Lyubartsev, *Chem. Eng. Sci.*, 2017, **174**, 174–188.
- 166 X. Huang, J. Lu, W. Wang, X. Wei and J. Ding, *Appl. Surf. Sci.*, 2016, **371**, 307–313.
- 167 G. Avci, I. Erucar and S. Keskin, *ACS Appl. Mater. Interfaces*, 2020, **12**, 41567–41579.
- 168 G. Avci, S. Velioglu and S. Keskin, *ACS Appl. Mater. Interfaces*, 2018, **10**, 33693–33706.
- 169 H. Fang, A. Kulkarni, P. Kamakoti, R. Awati, P. I. Ravikovitch and D. S. Sholl, *Chem. Mater.*, 2016, **28**, 3887–3896.
- 170 C. Shi, L. Li and Y. Li, *J. CO2 Util.*, 2020, **42**, 101346.

